Research Paper

MAEL in human cancers and implications in prognostication and predicting benefit from immunotherapy over VEGFR/mTOR inhibitors in clear cell renal cell carcinoma: a bioinformatic analysis

Jin Tao[1,*], Jinshan Cui[1,*], Yu Xu[2,*], Yafeng Fan[1,*], Guodong Hong[1], Qiaoxia Zhou[2], Guoqiang Wang[2], Leo Li[2], Yusheng Han[2], Chunwei Xu[3], Wenxian Wang[4], Shangli Cai[2], Xuepei Zhang[1]

[1]Department of Urology, The First Affiliated Hospital of Zhengzhou University, Zhengzhou, Henan, China
[2]Burning Rock Biotech, Guangzhou, Guangdong, China
[3]Institute of Basic Medicine and Cancer (IBMC), Chinese Academy of Sciences, Hangzhou, Zhejiang, China
[4]Department of Clinical Trial, The Cancer Hospital of the University of Chinese Academy of Sciences (Zhejiang Cancer Hospital), Hangzhou, Zhejiang, China
*Equal contribution

Correspondence to: Xuepei Zhang; **email:** zhangxuepei@263.net, https://orcid.org/0000-0003-0919-5871
Keywords: MAEL, pan-cancer analysis, clear cell renal cell carcinoma, prognosis, immunotherapy
Received: August 15, 2023 **Accepted:** December 13, 2023 **Published:** January 31, 2024

ABSTRACT

***Maelstrom* (*MAEL*), a novel cancer/testis-associated gene, may facilitate the initiation and progression of human malignancies, warranting comprehensive investigations. Single-cell and tissue-bulk transcriptomic data demonstrated higher *MAEL* expression in testis (spermatogonia/spermatocyte), kidney (proximal tubular cell), and brain (neuron/astrocyte), and corresponding cancers, including testicular germ cell tumor, glioma, papillary renal cell carcinoma, and clear cell renal cell carcinoma (ccRCC). Of these cancers, only in ccRCC did *MAEL* expression exhibit associations with both recurrence-free survival and overall survival. High *MAEL* expression was associated with an anti-inflammatory tumor immune microenvironment and VEGFR/mTOR activation in ccRCC tissues and high sensitivities to VEGFR/PI3K-AKT-mTOR inhibitors in ccRCC cell lines. Consistent with these, low rather than high *MAEL* expression indicated remarkable progression-free survival benefits from immune checkpoint inhibitor (ICI)-based immunotherapies over VEGFR/mTOR inhibitors in two large phase III trials (JAVELIN Renal 101 and CheckMate-025). *MAEL* is a biologically and clinically significant determinant with potential for prognostication after nephrectomy and patient selection for VEGFR/mTOR inhibitors and immunotherapy-based treatments.**

INTRODUCTION

Maelstrom (*MAEL)*, located in 1q24, is an evolutionarily conserved gene first found in *Drosophila* oocyte [1]. The full-length MAEL protein contains a high-mobility group (HMG) domain for DNA binding as well as a novel MAEL-specific domain with a single-stranded RNA (ssRNA)-specific endonuclease activity [2–4]. *MAEL* expression has been discovered by Northern blot in only the testis of normal human tissues [5], while it has been found to be aberrant in numerous cancer cell lines [5, 6]. Unlike in germ cells, where MAEL is a nuage component involved in posttranscriptional piRNA-mediated transposon silencing [7], MAEL has been identified as a component of stress granule (SG) in tumor cells [8], relating to the cellular response to abnormal physiological or pathological conditions, such as hypoxia, oxidative stress, and chemotherapeutic drugs [9].

As a novel cancer/testis-associated gene, *MAEL* is deemed to participate in stem cell self-renewal that favors tumor proliferation [10]. Emerging evidence has revealed its oncogenic mechanisms in cell lines concerning the cancers in breast [6], esophagus [11], stomach [12], colorectum [13], liver [6, 14], ovary [6, 15], and bladder [16], in terms of inducing epithelial-mesenchymal transition (EMT) [11–15], protecting genetic integrity [6], and recruiting myeloid-derived suppressor cells (MDSCs) that leads to an anti-inflammatory tumor immune microenvironment (TIME) [11]. Given the associations of *MAEL* with EMT/stemness and TIME, we hypothesized that MAEL might define a stemness-like and immune-suppressive phenotype associated with the resistance to immune checkpoint inhibitors (ICIs).

In this study, we first delineated the expression landscape of *MAEL* in human normal tissues and cancers, finding high *MAEL* expression in normal tissues such as testis (spermatogonia/spermatocyte), kidney (proximal tubular cell), and brain (neuron/astrocyte), as well as cancers including testicular germ cell tumor (TGCT), glioma, papillary renal cell carcinoma (pRCC), and clear cell renal cell carcinoma (ccRCC). Of these cancers, only in ccRCC did *MAEL* expression appear to be associated with both recurrence-free survival (RFS) and overall survival (OS). In two large phase III trials, JAVELIN Renal 101 and CheckMate-025, high *MAEL* expression was linked with anti-inflammatory TIME and VEGFR/mTOR activation in ccRCC tissues, high sensitivities to VEGFR/PI3K-AKT-mTOR inhibitors in ccRCC cell lines, and poor progression-free survival (PFS) benefits from ICI-based immunotherapies over VEGFR/mTOR inhibitors.

MATERIALS AND METHODS

Study design and clinical cohorts

In total, there are six parts in our study, including (i) *MAEL* expression in normal tissues (tissue bulk RNA-seq, Human Protein Atlas [HPA]) and cells (single cell RNA-seq, data source: Supplementary Table 1) [17–19], (ii) *MAEL* mRNA expression in 32 types of cancer cell lines (Cancer Cell Line Encyclopedia [CCLE]) and 33 types of cancer tissues (The Cancer Genome Atlas [TCGA]) and its pan-cancer prognostic effects [20, 21], (iii) mRNA expression of the six transcripts of *MAEL* among 33 cancer types and its association with DNA methylation and copy number variations (CNVs) [22, 23], (iv) protein expression of MAEL in ccRCC in the HPA database [18] and mRNA expression of *MAEL* in patient-derived xenografts (GSE83820 and GSE36895) [24, 25], (v) associations of *MAEL* expression with clinicopathological features, mutations, gene expression, and prognosis in The Cancer Genome Atlas-Kidney Renal Clear Cell Carcinoma (TCGA-KIRC) cohort (n=522) [26] and the International Cancer Genome Consortium (ICGC)-Pan-cancer analysis of whole genomes (PCAWG) Renal Cell Carcinoma-Europe (RECA-EU) cohort (n=64) [27, 28], (vi) association between *MAEL* expression and sensitivities to VEGFR/mTOR inhibitors in the ccRCC cell lines of the Genomics of Drug Sensitivity in Cancer (GDSC, n=16) dataset [29] and patients with advanced ccRCC treated with first-line sunitinib (E-MTAB-3267, n=53) [30], and (vii) implications of *MAEL* expression in predicting the benefit from ICI-based therapies over VEGFR/mTOR inhibitors in the JAVELIN Renal 101 trial (phase III, avelumab+axitinib vs. sunitinib, n=726) and the CheckMate-025 trial (phase III, nivolumab vs. everolimus, n=250) [31].

The basic features of these clinical cohorts, including sample sizes, outcomes, clinical settings, the platforms of RNA-seq and immunohistochemical (IHC) staining of programmed cell death-ligand 1 (PD-L1), and treatment, are displayed in Supplementary Table 2. This report follows the Strengthening the Reporting of Observational Studies in Epidemiology (STROBE) and the REporting recommendations for tumour MARKer prognostic studies (REMARK) reporting guidelines.

Genomic analysis

The genomic alterations of the TCGA-KIRC cohort were downloaded from the University of California Santa Cruz (UCSC) Xena database [32]. Tumor mutational burden (TMB) and intratumoral heterogeneity (ITH) were retrieved from the TCGA pan-cancer article [26]. The Catalogue Of Somatic Mutations In Cancer (COSMIC) database was used as a supplement to the TCGA-KIRC cohort for measuring the mutational rate of *MAEL* in ccRCCs. Silent mutations were excluded from our study. The genomic locations of the six transcripts of *MAEL* and their regulation regions (e.g., promoter and enhancer) were illustrated using the Ensembl [33].

Transcriptomic analysis

MAEL expression in normal human tissue bulks and single cells was illustrated using the HPA (https://www.proteinatlas.org/ENSG00000143194-MAEL, for details, see Supplementary Methods) [17–19]. For tissue bulk RNA-seq, there are 107 samples of the nervous system (e.g., cerebral cortex) in the HPA dataset, and we used the median value to represent the *MAEL* expression in the nervous system. For single-cell RNA-seq, Uniform

Manifold Approximation and Projection (UMAP) was used to visualize the different single-cell clusters, and the cell type of each cluster was determined by the expression of cell-type markers.

The expression of the six isoforms of *MAEL* in cancer tissue bulks and the prognostic effects of *MAEL* expression in the 33 cancer types of the TCGA database were analyzed using the Gene Expression Profiling Interactive Analysis 2 (GEPIA2, http://gepia2.cancer-pku.cn) [21]. The association between *MAEL* expression and its DNA methylation level was explored using the MEXPRESS (https://mexpress.be/index.html) [22, 23]. The level of transcriptomic data was measured by $\log_2$(transcripts per kilobase million [TPM]+1) in the present study.

Gene Ontology (GO) analysis was performed on the website (http://geneontology.org/) by using the annotation data set named Protein Analysis Through Evolutionary Relationships (PANTHER) GO-slim biological process [34, 35].

For Gene Set Enrichment Analysis (GSEA), the javaGSEA Desktop Application (GSEA 4.0.1) was used to investigate the gene signatures significantly enriched in the ccRCC samples with higher or lower *MAEL* expression (cut-off: median value) [36]. The normalized enrichment score (NES) is the primary statistic for assessing the enrichment of gene sets.

Pharmacogenomic analysis

In total, 16 ccRCC cell lines with data on transcriptomics and sensitivities to anti-cancer agents were included for analysis. For each targeted agent, the half-maximal inhibitory concentration levels (IC_{50}) of 16 ccRCC cell lines were scaled according to their geomean (formula: lg[IC_{50}/geomean]). Two-way analysis of variance was used to assess the difference in sensitivities between the cell lines with high and low *MAEL* expression.

Statistical analysis

To assess the between-group difference, we used (i) the Fisher exact test for categorical variables, (ii) the Mann-Whitney test, t test with Welch correction, the Kruskal-Wallis test, or one-way analysis of variance for continuous variables, and (iii) the Kaplan-Meier (KM) curves, the Log-rank test, and the Cox proportional-hazards regression model (hazard ratio [HR] and 95% confidence interval [CI]) for time-to-event variables. The variables with a p-value below 0.05 in the uni-variable Cox regression were included in the following multivariable Cox model. The spearman or Pearson correlation was used to test the correlations between continuous variables.

The statistical analyses were performed using IBM SPSS Statistics 22 or R 4.1.3. The nominal level of significance was set at 5%, and all 95% CIs were 2-sided unless otherwise specified. The adjusted P-value (Q-value) was calculated using the Benjamini-Hochberg method.

Data availability

The authors declare that relevant data supporting the findings of this study are available within the paper and its Supplementary Files. Due to ethical and privacy concerns, we are unable to publish the patient-level data in our study, of which readers may contact the corresponding authors for the access for non-commercial purposes.

RESULTS

MAEL expression in normal tissues and single cells

A previous study observed that human MAEL expression was exclusive in testis rather than other tissues, including brain, heart, liver, lung, spleen, kidney, and ovary as determined by Northern blot (5). Here, we analyzed the RNA-seq data of 32 kinds of human tissues. Besides testis, relatively higher MAEL expression was revealed in placenta, heart muscle, epididymis, kidney, and nervous system (e.g., brain and spinal cord; Figure 1A and Supplementary Table 3).

We further analyzed the single-cell transcriptomes of 25 kinds of human tissues and peripheral blood mono-nuclear cells (PBMCs) to assess the expression level of *MAEL* in different cell types (Supplementary Table 4). As for the tissues with higher *MAEL* expression (testis, placenta, heart muscle, kidney, and brain), the UMAP plots and *MAEL* expression in each single cell cluster are shown in Figure 1B–1E and Supplementary Figure 1, and the corresponding mRNA expression of cell-type markers in different single cell type clusters are displayed in Supplementary Figure 2–6, respectively. In short, *MAEL* was expressed relatively higher in early spermatids, spermatocytes, spermatogonia, and late spermatids in testis (Figure 1B), fibroblasts and endothelial cells in placenta (Figure 1C), smooth muscle cells and cardiomyocytes in heart muscle (Figure 1D), proximal tubular cells in kidney (Figure 1E), and astro-cyte, excitatory neurons, and oligodendrocyte precursor cells in brain (Supplementary Figure 1).

Of note, first, unlike the pattern in testis and placenta where *MAEL* was expressed "equivalently" in the

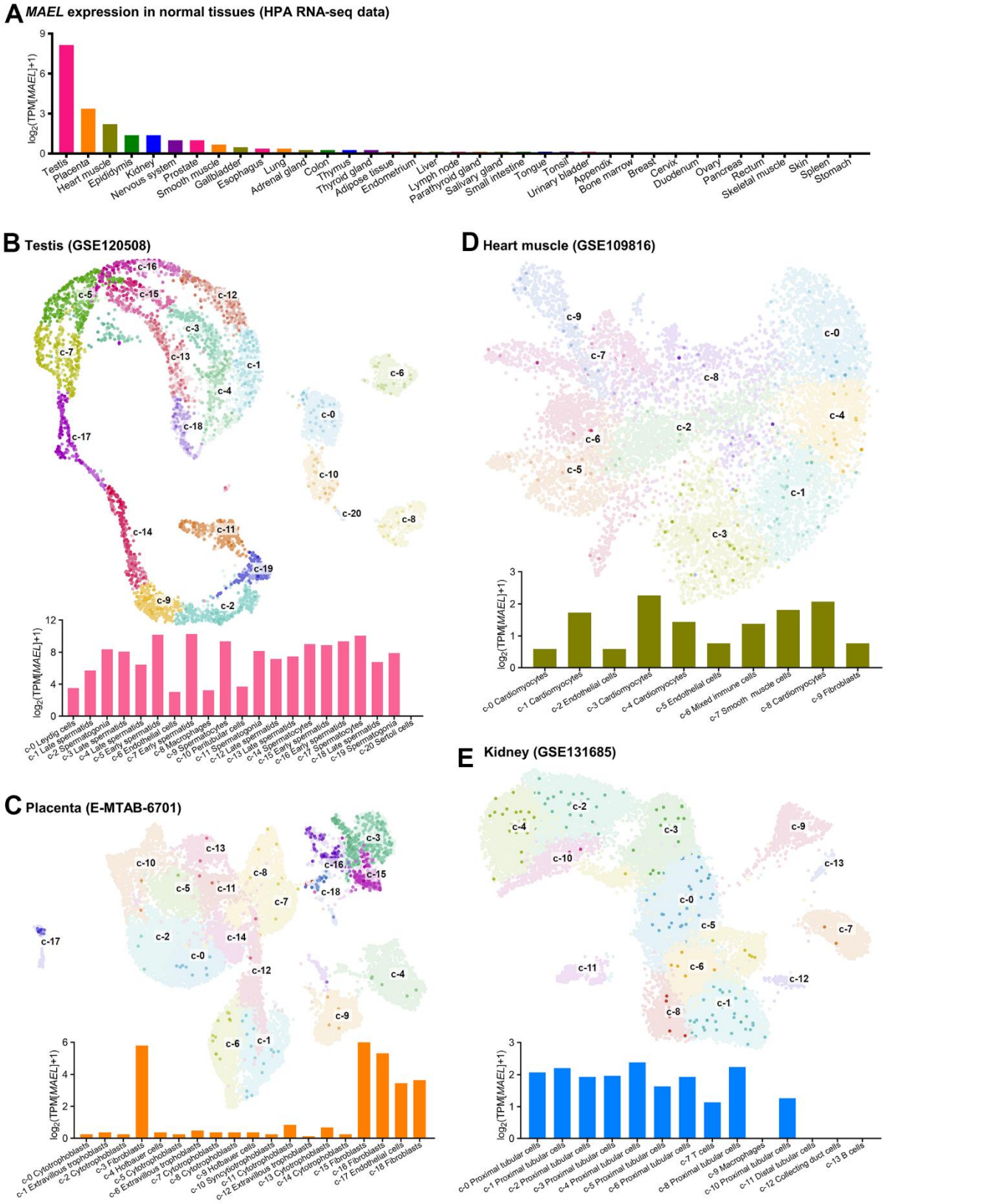

Figure 1. *MAEL* expression in normal tissues and single-cell clusters. (**A**) *MAEL* expression in normal tissues (tissue bulk RNA-seq, Human Protein Atlas). (**B**–**E**) UMAP plots and *MAEL* expression in the single cell clusters (single cell RNA-seq) of testis (GSE120508, **B**), placenta (E-MTAB-6701, **C**), heart muscle (GSE109816, **D**), and kidney (GSE131685, **E**). The depth of the color of each point reflects the relative expression of *MAEL*. Abbreviations: TPM=transcripts per kilobase million, UMAP=Uniform Manifold Approximation and Projection.

single-cell clusters with higher *MAEL* expression (e.g., c-7 in testis and c-15 in placenta, Figure 1B, 1C), *MAEL* was expressed "sporadically" in the proximal tubular cells in kidney (Figure 1E), suggesting that *MAEL* might function in a certain subset of proximal tubular cells, probably relevant to the homeostasis of proximal tubule. Second, *MAEL* expression was extremely low in immune tissues (lymph node, spleen, bone marrow, and thymus, Figure 1A) and the immune cell clusters in other tissues and peripheral blood (Supplementary Table 4), raising the possibility that MAEL might not be involved in the maturation and activation of immune cells.

MAEL in cancer tissues and cancer cell lines

Among the 33 cancer types in the TCGA database (abbreviations, see Supplementary Table 5), *MAEL* was expressed higher in TGCT, glioblastoma multiforme (GBM), brain lower-grade glioma (LGG), kidney renal papillary cell carcinoma (KIRP, also abbreviated as pRCC), and KIRC (also abbreviated as ccRCC; Figure 2A). These results were consistent with its expression in normal cell types. For instance, unlike pRCC and ccRCC originating from proximal tubular cells with high *MAEL* expression (Figure 1E), kidney chromophobe carcinoma (KICH) develops from distal tubular cells that did not express *MAEL* (Figure 1E) and had far lower expression of *MAEL* than KIRC and KIRP (Figure 2A). Similarly, in the CCLE database (abbreviations, see Supplementary Table 5), high *MAEL* expression was observed in nervous system tumors and KIRC (Figure 2B).

As for prognostic value, the RFS and OS of two subgroups divided by the median *MAEL* mRNA level

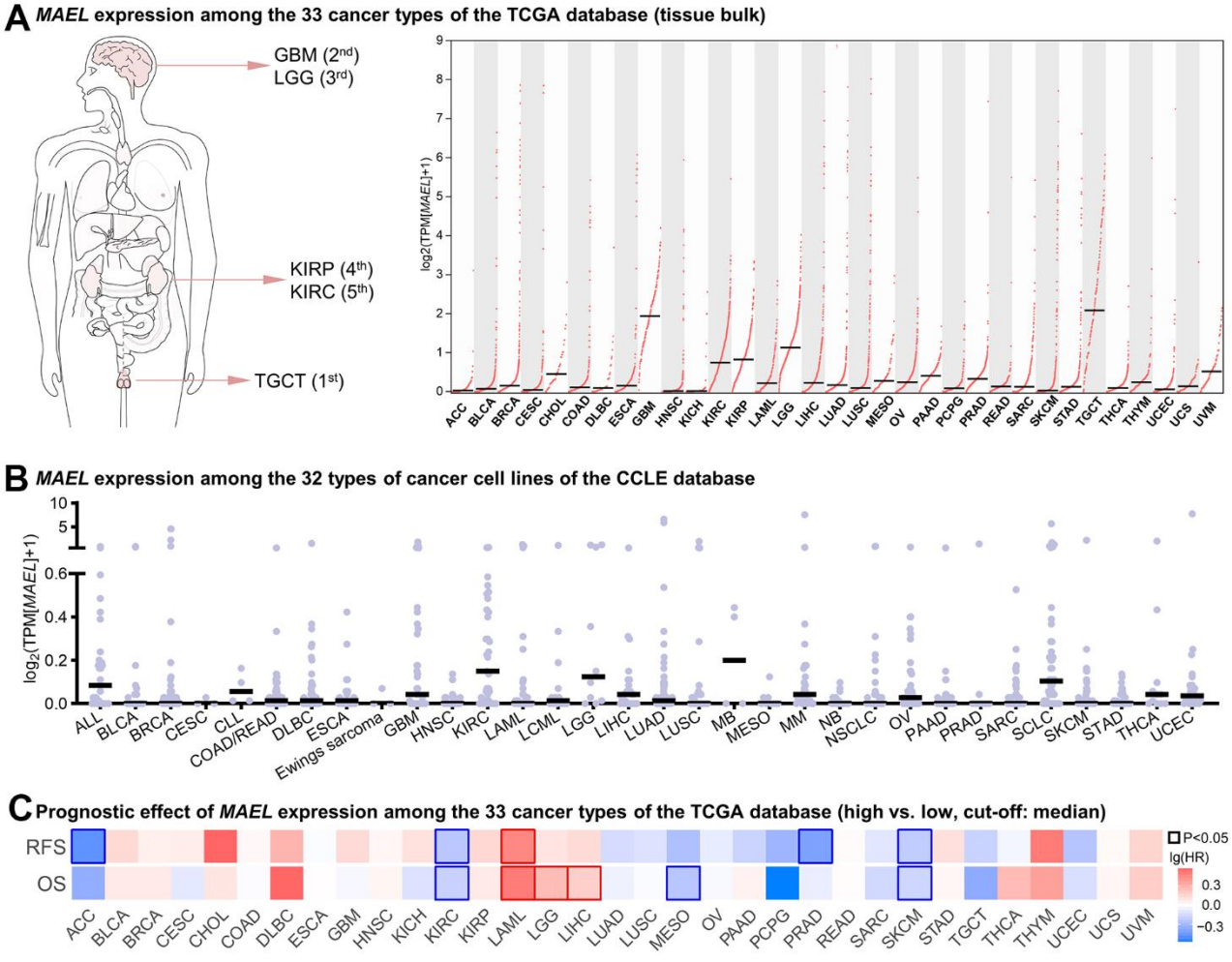

Figure 2. Pan-cancer analysis of *MAEL*. (**A**) *MAEL* expression among the 33 cancer types of the TCGA database (tissue bulk RNA-seq). (**B**) MAEL expression among the 32 types of cancer cell lines of the CCLE database. (**C**) Prognostic effect of *MAEL* expression among the 33 cancer types of the TCGA database (high vs. low, cut-off: median). Abbreviations: CCLE=Cancer Cell Line Encyclopedia, TCGA=The Cancer Genome Atlas.

were compared among the 33 cancer types in the TCGA database. Consistent prognostic effects for predicting both RFS and OS (P<0.05) were observed in KIRC, acute myeloid leukemia (LAML), and skin cutaneous melanoma (SKCM, Figure 2C).

Given the level of *MAEL* mRNA and its prognostic effect, MAEL may play a crucial role in KIRC, compared with other cancer types. We sought to further discover its linkages with clinicopathological features, DNA methylation, genomic alterations, pathway activation, drug sensitivity, and immunotherapy efficacy in clear cell renal cell carcinomas.

Expression of the six transcripts of *MAEL* and its potential regulatory mechanisms in ccRCCs

MAEL, located in chromosome 1 (166,975,582-167,022,214), has six transcripts, of which *MAEL-204* and *MAEL-205* are processed transcripts, and the other four transcripts (*MAEL-206*, *MAEL-201*, *MAEL-202*, and *MAEL-203*) can be translated into proteins (Figure 3A; features of these isoforms are shown in Supplementary Table 6). In particular, MAEL-206 lacks the HMG domain compared with MAEL-201, 202, and 203 (Figure 3A).

The expression of these six transcripts in the 33 cancer types in the TCGA database is shown in Supplementary Figure 7. Among the five cancer types with the highest *MAEL* expression, TGCT had equivalent expression levels of *MAEL-206* and *MAEL-202*, while the *MAEL* expression in the other four cancer types was dominated by *MAEL-206* (>90%, Figure 3B), indicating the potential role of *MAEL-206* in brain and kidney tumors.

Given the distinct expression patterns of *MAEL* isoforms in KIRC and TGCT, we further explored the DNA methylation level of *MAEL* and its association with mRNA expression in these two cancers. First, in KIRCs where *MAEL* expression was dominated by *MAEL-206*, *MAEL* expression was negatively correlated with the methylation level of cg08348962 near the promoter of *MAEL-206* (P=0.049), while this association was non-significant in TGCTs (P=0.24; Figure 3C and Supplementary Table 7, marked in blue). Second, compared with KIRCs, TGCTs had higher *MAEL-202* expression and lower methylation levels in the regions near its promoters (Figure 3C, marked in green); the methylation levels of these regions were negatively correlated with *MAEL* expression in TCGTs instead of KIRCs (P<0.05 in TCGTs and P>0.20 in KIRCs; Supplementary Table 7, marked in green). These results indicate that DNA methylation may, in part, explain the distinct expression patterns of *MAEL* isoforms in human cancers.

In addition to DNA methylation, copy number and mutation may affect transcription. *MAEL* expression was positively correlated with copy number (P<0.001, Supplementary Table 7). No mutational event of *MAEL* was observed in the ccRCCs of the TCGA and the COSMIC databases, suggesting that its function in ccRCCs might be regulated by expression level instead of the mutant protein.

Clinicopathological and prognostic correlates of *MAEL* in ccRCCs

Age, sex, race, and pathological TNM stage were not significantly associated with *MAEL* expression, while the samples with a poor histological grade had lower *MAEL* expression (P=0.022, Figure 3D and Supplementary Table 7). We further calculated the prognostic effect between *MAEL* expression and OS at each cut-off value ranging from 20th to 80th percentiles and observed that high *MAEL* expression trended to be associated with long OS at most cut-off values (Figure 3E). When the cut-off was empirically determined as the median value, the HR was 1.50 (low vs. high: 95% CI 1.11–2.03, P=0.008, Figure 3E). The prognostic effect of *MAEL* expression was independent of covariates including age, laterality, TNM stage, and histological grade (multivariable HR=1.54, 95% CI 1.13–2.09, P=0.006, Figure 3F). A similar association with RFS was also observed (univariable HR=1.43, 95% CI 1.00–2.04, P=0.050; multivariable HR=1.47, 95% CI 1.03–2.11, P=0.034; Supplementary Figure 8). In a small cohort retrieved from the ICGC-PCAWG RECA-EU database (n=64) [27, 28], we also observed a prognostic trend with similar HR (low vs. high: HR=1.58, 95% CI 0.70–3.58, P=0.28; Supplementary Figure 9).

MAEL protein expression in the cytoplasm of partial tumor cells was observed in two ccRCC samples of the HPA database using immunohistochemical staining (Supplementary Figure 10) [18]. This distribution profile is consistent with previous studies in hepatocellular carcinoma [14], ovarian cancer [15], bladder urothelial carcinoma [16], and colorectal adenocarcinoma [13]. Moreover, in the GSE83820 dataset including five ccRCC samples and their PDXs, compared to the primary grafts, the *MAEL* expression was increased at early passages (passage 1 [P1] vs. P0: P=0.014; P2 vs. P0: P=0.086) and tended to return to the baseline level at P4 (Supplementary Figure 11). A similar trend was observed in another PDX dataset (GSE36895, Supplementary Figure 11). These results indicate the stable expression of *MAEL* in ccRCC and suggest that MAEL might be involved in clonal evolution and/or immune escape during the early phase of xenograft development.

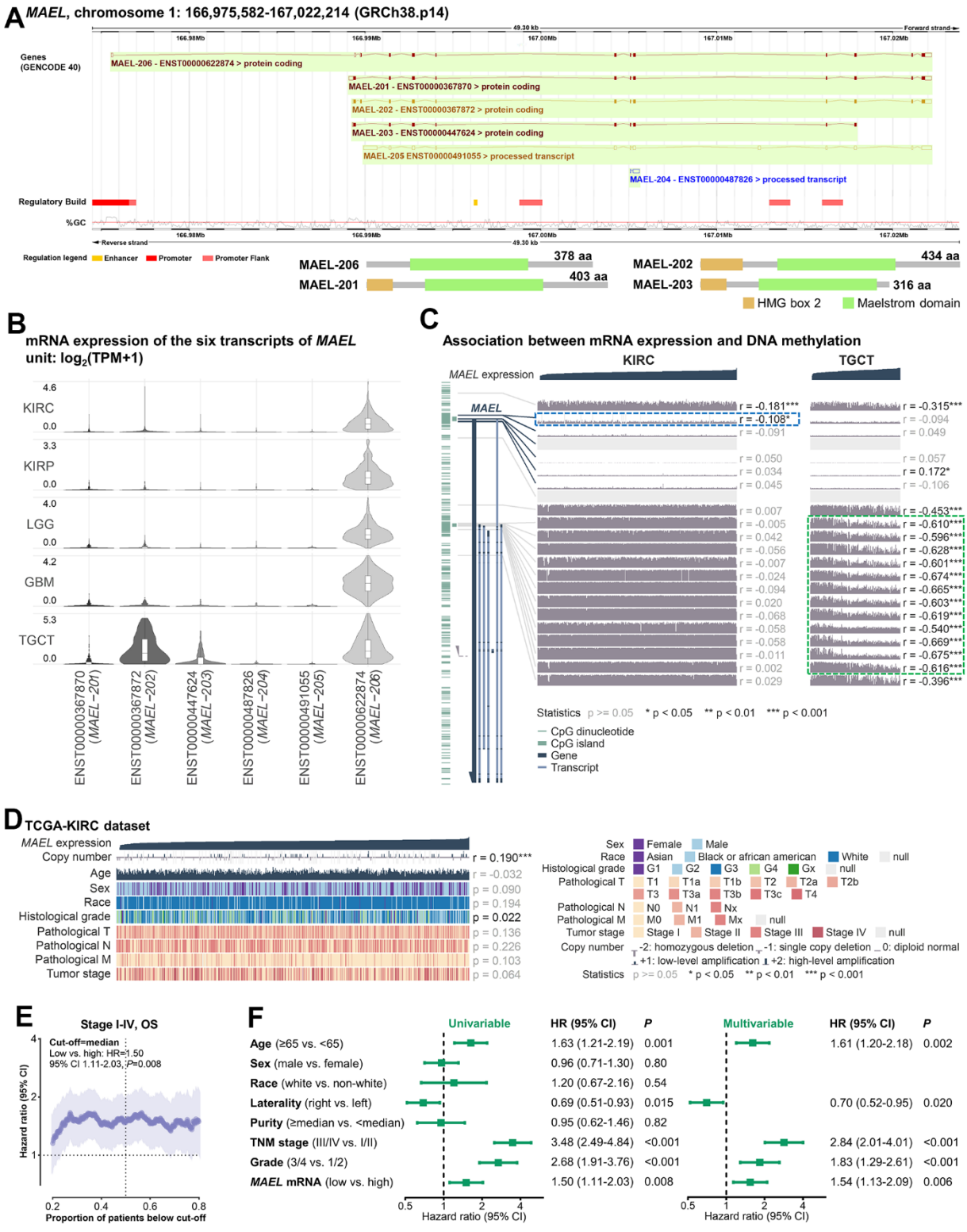

Figure 3. Expression and prognostic effect of *MAEL* in ccRCC. (**A**) Location of *MAEL* in human genome. (**B**) mRNA expression of the six transcripts of *MAEL* in the KIRCs, KIRPs, LGGs, GBMs, and TGCTs of the TCGA database. (**C**) Association between mRNA expression and DNA methylation in the KIRCs and TGCTs of the TCGA database. (**D**, **E**) Associations of *MAEL* expression with copy number, clinicopathological features (**D**) and overall survival (**E**) in the TCGA-KIRC cohort. (**F**) Univariable and multivariable analysis of the prognostic effect of *MAEL* expression in the TCGA-KIRC cohort. Abbreviations: ccRCC=clear cell renal cell carcinoma, GBM=glioblastoma multiforme, KIRC=Kidney Renal Clear Cell Carcinoma, KIRP=kidney renal papillary cell carcinoma, LGG=brain lower grade glioma, TCGA=The Cancer Genome Atlas, TGCT=testicular germ cell tumors.

MAEL was expressed higher in ccRCCs than in normal kidneys (P=0.024, Supplementary Figure 12) indicating its oncogenic role in ccRCC, while higher *MAEL* expression was associated with a better prognosis. This observation might seem counterintuitive. However, different types of ccRCCs may depend on different oncogenes, and *MAEL*-dependent ccRCCs may progress more slowly than those dependent on other oncogenes, thus exhibiting a relatively better prognosis.

Genomic, transcriptomic, and pharmacogenomic correlates of *MAEL* in ccRCCs

In the TCGA-KIRC cohort, *MAEL* expression was not associated with mutational count (P=0.99) or fraction genome altered (P=0.27). As for commonly mutated genes, high *MAEL* expression was associated with the mutations in *VHL*, *PBRM1*, and *SETD2* (P<0.05, Figure 4A), suggesting its linkage with activated angiogenesis [37, 38].

We further analyzed the correlations between *MAEL* expression and other genes' expression levels and identified 2,576 positively-correlated genes and 2,904 negatively-correlated genes (Figure 4B and Supplementary Table 8). The positively-correlated genes were enriched in the pathways concerning blood vessel development and Ras protein signal transduction (Q<0.05, Figure 4C) and excluded in the immune-related pathways about B cell, immunoglobulin-mediated immune response, lymphocyte activation, and complement activation (Q<0.05; Figure 4C, marked in bold). On the contrary, the negatively-correlated genes were enriched in the immune-related pathways relating to lymphocyte proliferation, inflammatory response, and cytokine (Q<0.05; Figure 4D, marked in bold).

Inhibitors of vascular endothelial growth factor receptor (VEGFR, e.g., sunitinib and axitinib) and mTOR (e.g., everolimus) exhibit anti-tumor activity in ccRCCs [39–41], largely due to the activation of angiogenesis and the PI3K-AKT-mTOR signaling [42–45]. Compared with the ccRCCs with low *MAEL* expression (below median), VEGF and mTOR signatures were enriched in those with high *MAEL* expression (VEGF: NES=2.28, P<0.001; mTOR: NES=1.68, P=0.013; Figure 4E). Among the 16 ccRCC cell lines in the CCLE database, the IC_{50} values of VEGFR and PI3K-AKT-mTOR inhibitors were lower in those with high *MAEL* expression than those with low *MAEL* expression (above median; P<0.001, Figure 4F and Supplementary Table 9). In the E-MTAB-3267 cohort including 53 patients with advanced ccRCC [30], high *MAEL* expression trended to be linked with favorable PFS on first-line sunitinib (high vs. low: HR=0.56, 95% CI 0.30–1.06, P=0.064, Supplementary Figure 13).

Taken together, *MAEL* expression was associated with inactivated anti-tumor immunity, activated pathways concerning VEGFR and PI3K-AKT-mTOR, and sensitivities to VEGFR/PI3K-AKT-mTOR inhibitors in ccRCCs.

***MAEL* expression predicts the benefits from ICI-based therapies over VEGFR/mTOR inhibitors in advanced/metastatic ccRCCs**

We further investigated the association of *MAEL* expression with the benefit from ICI-based therapies over VEGFR/mTOR inhibitors in two large phase III trials, the JAVELIN Renal 101 (avelumab plus axitinib vs. sunitinib) and the CheckMate-025 (nivolumab vs. everolimus).

First, the 726 advanced/metastatic ccRCC patients with available RNA-seq data in the JAVELIN Renal 101 trial (clinicopathological features, see Figure 5A) were randomly separated into a training set (n=484) and a validation set (n=242) with a ratio of 2:1. The difference in the association of a biomarker with survival across treatment arms is the essential proof of its predictive utility [46]. In the training set, for each cut-off value ranging from 20^{th} to 80^{th} percentiles, we calculated the treatment effect in the below cut-off and the above cut-off subgroups. The treatment effect was larger in the low *MAEL* group than the high *MAEL* group at all cut-offs (Figure 5B). The difference in treatment effect between these two subgroups reached its maximum at the cut-off of 67.4^{th} percentile (interaction HR=0.54, 95% CI 0.32–0.93, P=0.027, Figure 5B). At this cut-off, the benefit from avelumab plus axitinib over sunitinib was considerable in the low *MAEL* expression group (HR=0.53, 95% CI 0.38–0.73, P<0.001) while negligible in the high *MAEL* expression group (HR=0.97, 95% CI 0.63–1.49, P=0.87, Figure 5C). Comparable results were observed in the validation set (low *MAEL* expression group: HR=0.61, 95% CI 0.40–0.92, P=0.016; high *MAEL* expression group: HR=1.01, 95% CI 0.47–2.15, P=0.98, Figure 5D).

In the total set of all 726 patients, the interaction effect between *MAEL* expression and treatment effect was significant (interaction HR=0.56, 95% CI 0.36–0.88, P=0.012, Figure 5E). In the multivariable analysis using the data provided by the JAVELIN Renal 101 researchers, the interaction effect remained significant (multivariable interaction HR=0.58, 95% CI 0.37–0.91, P=0.019, Table 1). Compared with the low *MAEL* expression group, the high *MAEL* expression group had more females (P=0.001) and the m1/4 cluster defined by the TCGA Research Network study (P<0.001) [47], lower CD8 densities in tumor center (P=0.044) and total

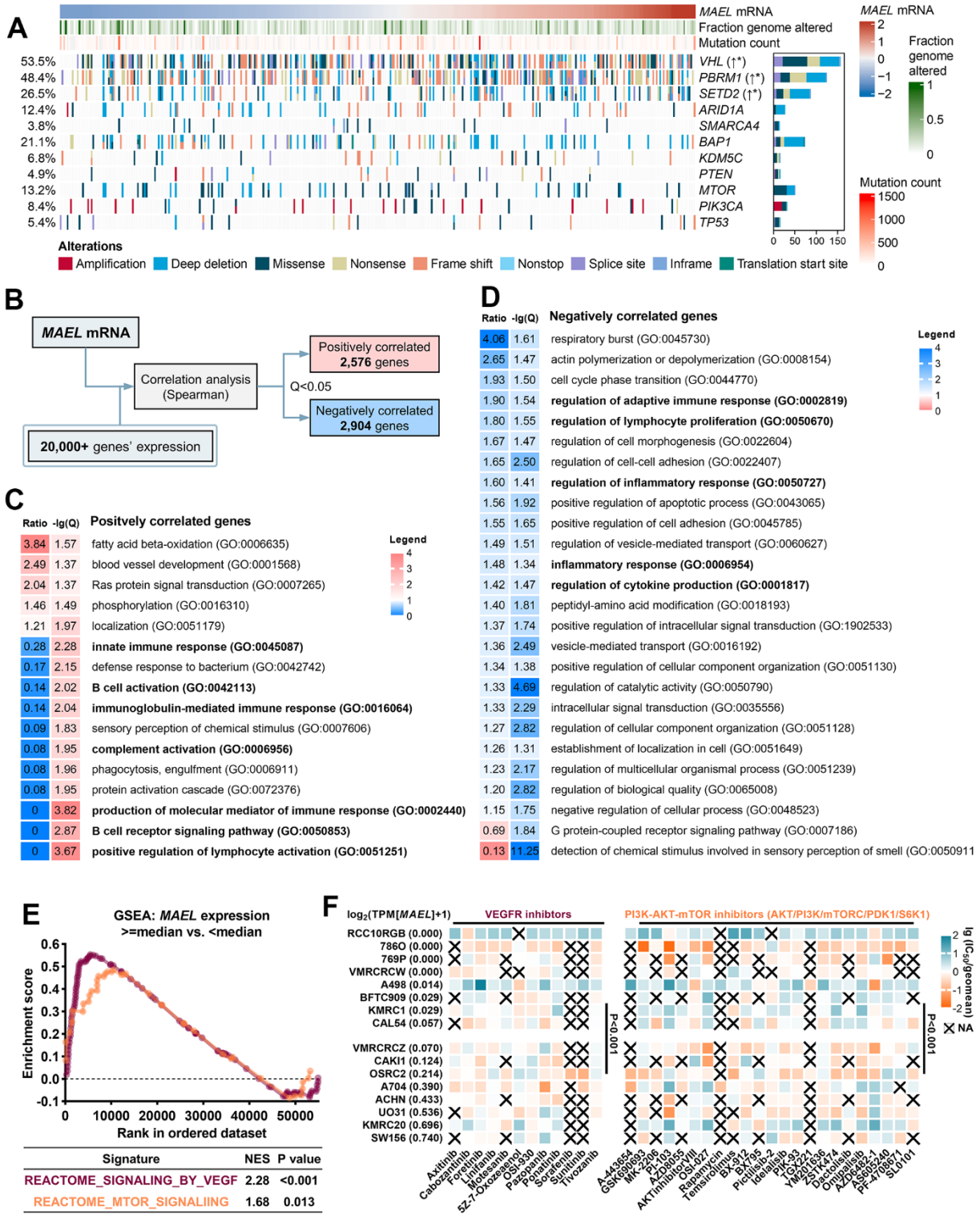

Figure 4. Associations of the *MAEL* expression with genomic alterations, gene expression, and sensitivities to VEGFR and PI3K-AKT-mTOR inhibitors. (**A**) Oncoprint illustrating the association between *MAEL* expression and genomic indices and alterations in the TCGA-KIRC cohort. (**B**) Diagram of identifying the genes with expression correlated with *MAEL* expression in the TCGA-KIRC cohort. (**C**, **D**) Gene Ontology results of the positively correlated genes (**C**) and negatively correlated genes (**D**). (**E**) Gene Set Enrichment Analysis results revealing the associations between *MAEL* expression (high vs. low, cut-off: median) and the enrichments of VEGF- and mTOR-related genes in the TCGA-KIRC cohort. (**F**) *MAEL* expression and its associations with the half-maximal inhibitory concentration levels in the 16 ccRCC cell lines. Abbreviations: IC_{50}=half-maximal inhibitory concentration levels, TCGA-KIRC=The Cancer Genome Atlas-Kidney Renal Clear Cell Carcinoma.

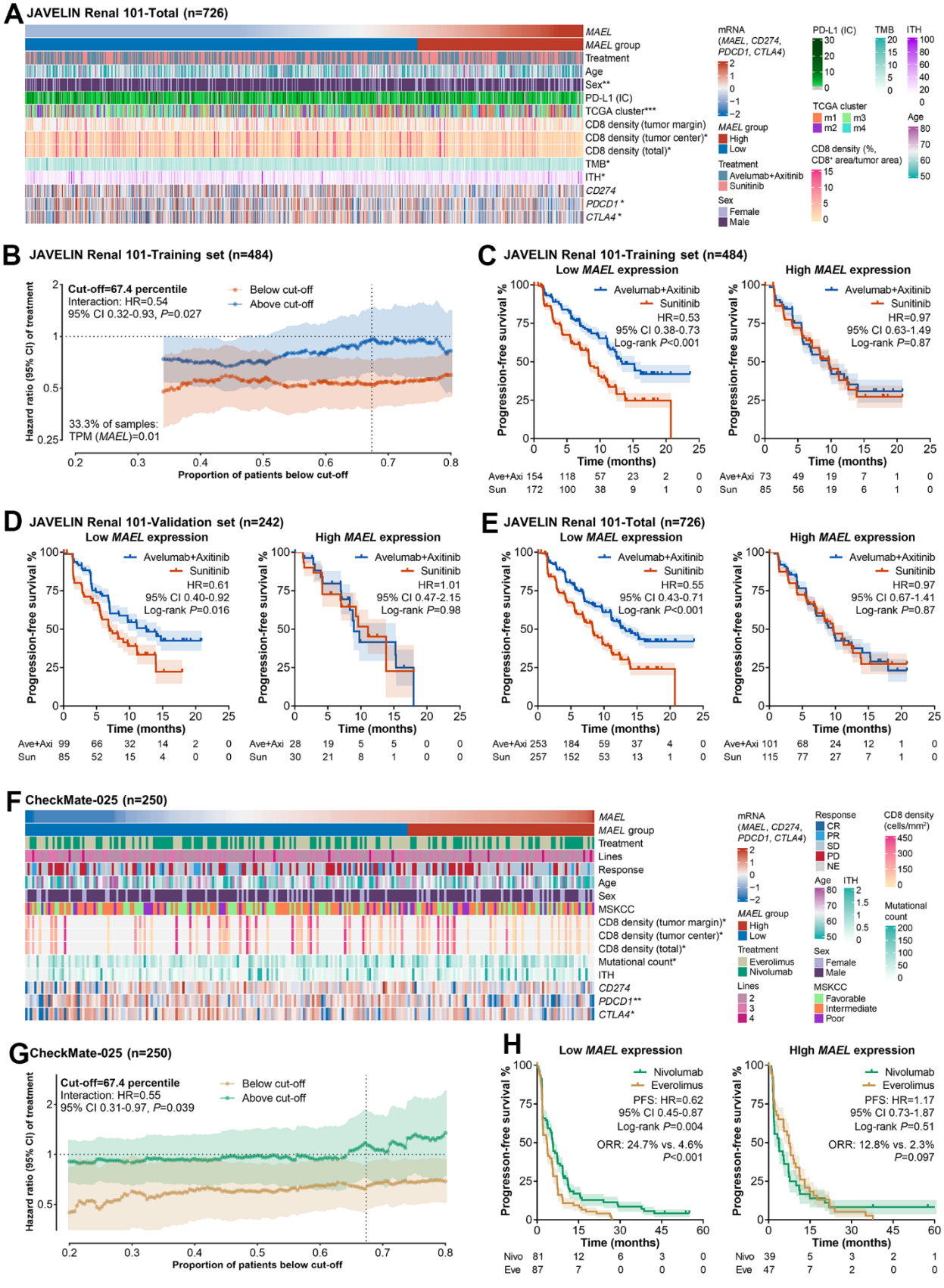

Figure 5. *MAEL* expression predicts the benefit from ICI-based immunotherapies over VEGFR/mTOR inhibitors in advanced/metastatic ccRCCs. (**A**) Heatmap illustrating *MAEL* expression and clinicopathological features of the JAVELIN Renal 101 cohort.

(**B**) The associations of the cut-off value with the treatment effect in the above- and the below-cut-off groups in the training set of the JAVELIN Renal 101 cohort. (**C–E**) The treatment effect (avelumab plus axitinib vs. sunitinib) in the low and the high *MAEL* expression groups in the training set (**C**), the validation set (**D**), and the total set (**E**) of the JAVELIN Renal 101 cohort. (**F**) Heatmap illustrating *MAEL* expression and clinicopathological features of the CheckMate-025 cohort. (**G**) The associations of the cut-off value with the treatment effect in the above- and the below-cut-off groups of the CheckMate-025 cohort. (**H**) The treatment effect (nivolumab vs. everolimus) in the low and the high *MAEL* expression groups of the CheckMate-025 cohort. Abbreviations: CI=confidence interval, CR=complete response, HR=hazard ratio, IC=immune cell, ITH=intratumoral heterogeneity, NE=not evaluable, ORR=objective response rate, PD=progressive disease, PD-L1=programmed cell death-ligand 1, PR=partial response, SD=stable disease, TCGA=The Cancer Genome Atlas, TMB=tumor mutational burden.

area (P=0.040), higher TMB (P=0.028) and ITH (P=0.022), and lower expression of *PDCD1* (P=0.010) and *CTLA4* (P=0.038, Figure 5A). Of note, *MAEL* expression was not associated with the *CD274* mRNA expression in tissue bulk (P=0.46) and the PD-L1 protein expression on immune cells (P=0.57, Figure 5A), indicating the irrelevance between the predictive utility of MAEL and PD-L1 expression.

In the CheckMate-025 trial involving 250 advanced/metastatic ccRCC patients with available RNA-seq data (Figure 5F), the curves of treatment effect in the "below cut-off" and "above cut-off" subgroups are shown in Figure 5G. The treatment effect was larger in the low *MAEL* group than the high *MAEL* group at all cut-offs (Figure 5G). At the cut-off (67.4^{th} percentile) derived from the training set of the JAVELIN Renal 101 cohort, the interaction effect was significant (HR=0.55, 95% CI 0.37–0.97, P=0.039, Figure 5G). Nivolumab delivered a significantly higher ORR and longer PFS than everolimus in the low *MAEL* expression subgroup (ORR: 24.7% vs. 4.6%, P<0.001; PFS: HR=0.62, 95% CI 0.45–0.87, P=0.004), but not in the high Notch-score subgroup (ORR: 12.8% vs. 2.3%, P=0.097; PFS: HR=1.17, 95% CI 0.73–1.87, P=0.51; Figure 5H). The interaction effect remained significant in the multivariable model (multivariable interaction HR=0.51, 95% CI 0.29–0.91, P=0.023, Table 1). High *MAEL* expression was associated with few $CD8^+$ T cells in tumor center (P=0.040), tumor margin (P=0.016), and total area (P=0.026), high TMB (P=0.013), and low expression of *PDCD1* (P=0.003) and *CTLA4* (P=0.049) rather than *CD274* (P=0.12, Figure 5F).

We further analyzed the association between *MAEL* expression and immune cell signatures in advanced/metastatic ccRCCs. In the three cohorts (JAVELIN, CheckMate, and TCGA), high *MAEL* expression was consistently linked with low levels of the signatures concerning activated B, $CD4^+$ T, $CD8^+$ T, and dendritic cells, central memory $CD4^+$ and $CD8^+$ T cells, effector memory $CD8^+$ T cell, immature B cell, macrophage, MDSC, natural killer T cell, regulatory T cell, and type I T helper cell (P<0.10, detailed statistics, see Figure 6A–6C), indicating an anti-inflammatory microenvironment.

Taken together, high *MAEL* expression was identified as an independent indicator of poor benefits from ICI-based therapies over VEGFR/mTOR inhibitors in advanced ccRCCs, potentially mediated by tumor-infiltrating immune cells and the expression of PD-1 and CTLA-4 rather than PD-L1.

DISCUSSION

In this study, we first delineated the expression landscape of *MAEL* in human normal tissues and cancers. Given that *MAEL* was highly expressed and was associated with both RFS and OS in ccRCCs, we investigated its implications in this cancer type in depth. High *MAEL* expression was associated with anti-inflammatory TIME, enhanced VEGFR and mTOR activities, and high sensitivities to VEGFR/PI3K-AKT-mTOR inhibitors. In the two clinical trials, the PFS benefits from ICI-based therapies over VEGFR/mTOR inhibitors were minimal in the high *MAEL* expression group but significant in the low *MAEL* expression group.

In all tumors except TGCT, MAEL is dominated by the MAEL-206 isoform, which lacks the HMG domain in the N terminal compared to the full-length MAEL. This expression pattern may be partly controlled by the methylation levels of the promoters of different isoforms. So far, nearly all published MAEL-associated cancer studies have been conducted in non-TGCT cell lines using plasmids carrying the full-length human *MAEL* cDNA. It might be more appropriate to carefully discern the function of each MAEL isoform in cell line and animal studies.

MAEL, as a potential oncogene, was expressed higher in ccRCCs than in normal kidneys, while high *MAEL* expression was identified as an independent indicator of favorable prognosis. This observation might seem counterintuitive. However, different types of ccRCCs may depend on different oncogenes, and *MAEL*-dependent ccRCCs may progress more slowly than those dependent on other oncogenes, thus exhibiting a relatively better prognosis. This oncogenic and prognostic pattern was also observed in other SG genes associated with *MAEL*, such as G3BP stress granule assembly factor 1/2 (*G3BP1/2*) [21, 48], suggesting that

Table 1. Predictive effect of the *MAEL* expression in multivariable models.

Parameter	JAVELIN Renal 101: progression-free survival			
	Univariable analysis		Multivariable analysis	
	HR (95% CI)	P-value	HR (95% CI)	P-value
Age (≥65 vs. <65)	0.74 (0.60-0.93)	0.009	0.77 (0.61-0.96)	0.018
Sex (male vs. female)	0.90 (0.71-1.14)	0.38		
PD-L1 mRNA (≥median vs. <median)	0.91 (0.74-1.12)	0.37		
PD-L1 IC score (dummy variable)		0.43		
1-9 vs. 0	1.14 (0.90-1.44)	0.28		
>=10 vs. 0	1.23 (0.87-1.74)	0.25		
$CD8^+$ density (≥median vs. <median)				
Tumor center	0.95 (0.77-1.18)	0.67		
Tumor margin	1.03 (0.76-1.41)	0.83		
Total	0.93 (0.75-1.16)	0.52		
TMB (≥median vs. <median)	0.95 (0.76-1.17)	0.61		
ITH (≥median vs. <median)	1.15 (0.93-1.42)	0.20		
TCGA subtype (dummy variable)		0.013		0.024
2 vs. 1	1.01 (0.73-1.40)	0.93	1.07 (0.77-1.48)	0.70
3 vs. 1	1.52 (1.15-2.01)	0.004	1.53 (1.15-2.03)	0.003
4 vs. 1	1.20 (0.87-1.65)	0.26	1.16 (0.85-1.60)	0.35
NA vs. 1	0.82 (0.38-1.77)	0.61	0.93 (0.43-2.04)	0.86
Treatment (avelumab+axitinib vs. sunitinib)	0.98 (0.67-1.42)	0.91	0.98 (0.67-1.43)	0.92
MAEL expression (low vs. high)	1.23 (0.91-1.67)	0.19	1.16 (0.85-1.58)	0.34
Interaction between treatment and *MAEL* expression	**0.56 (0.36-0.88)**	**0.012**	**0.58 (0.37-0.91)**	**0.019**
Parameter	**CheckMate-009/010/025: progression-free survival**			
	Univariable analysis		**Multivariable analysis**	
	HR (95% CI)	**P-value**	**HR (95% CI)**	**P-value**
Age (≥65 vs. <65)	0.91 (0.69-1.19)	0.50		
Sex (male vs. female)	1.15 (0.85-1.55)	0.38		
PD-L1 mRNA (≥median vs. <median)	1.00 (0.77-1.30)	0.99		
MSKCC risk (dummy variable)		0.019		0.010
Intermediate vs. favorable	1.14 (0.84-1.53)	0.40	1.21 (0.90-1.64)	0.21
Poor vs. favorable	1.69 (1.17-2.46)	0.006	1.78 (1.22-2.59)	0.003
CD8+ density				
Tumor center (≥median vs. <median)	1.11 (0.65-1.89)	0.70		
Tumor margin (≥median vs. <median)	1.21 (0.72-2.05)	0.48		
Total (≥median vs. <median)	1.11 (0.65-1.89)	0.71		
Treatment lines (dummy variable)		0.73		
3 vs. 2	1.11 (0.83-1.49)	0.47		
4 vs. 2	1.14 (0.63-2.05)	0.67		
TMB (≥median vs. <median)	1.09 (0.79-1.51)	0.58		
ITH (≥median vs. <median)	1.05 (0.75-1.46)	0.79		
Treatment (nivolumab vs. everolimus)	1.15 (0.72-1.83)	0.57	1.17 (0.73-1.86)	0.51
MAEL expression (low vs. high)	1.62 (1.10-2.39)	0.014	1.66 (1.13-2.45)	0.011
Interaction between treatment and *MAEL* expression	**0.55 (0.31-0.97)**	**0.039**	**0.51 (0.29-0.91)**	**0.023**

Abbreviations: CI, confidence interval; HR, hazard ratio; IC, immune cell; ITH, intratumoral heterogeneity; MSKCC, memorial sloan-kettering cancer center; NA, not applicable; PD-L1, programmed cell death-ligand 1; PFS, progression-free survival; TMB, tumor mutational burden.

the MAEL/SG-dependent ccRCCs might progress more slowly compared with other ccRCCs.

In ccRCC, high *MAEL* expression was associated with VEGFR/mTOR activation and an anti-inflammatory TIME, which can explain the high sensitivities to VEGFR/PI3K-AKT-mTOR inhibitors and the poor benefit from ICI-based therapies over VEGFR/mTOR inhibitors. The associations of MAEL with AKT activation and a suppressive TIME have been disclosed in the cell lines of hepatocellular carcinoma and esophageal squamous cell carcinoma [11, 14]. The interaction between a biomarker and treatment effect (difference in the association of a biomarker with survival across treatment arms) is the essential proof of its predictive utility [46]. The interaction effects between *MAEL* expression and treatment choice in the two phase III trials were both significant, implying that, compared to VEGFR/mTOR inhibitors, ICI-based immunotherapies might be recommended for the ccRCCs with low *MAEL* expression. Due to the lack of patient-level data, it is not available to validate our results in other trials, e.g., CheckMate-214 and IMmotion151 [49, 50].

As for limitations, first, the molecular correlates of *MAEL* were analyzed using bioinformatic methods in our study. Biological validation using cell lines and xenograft models is warranted. Here, *MAEL* expression and its association with the sensitivity of VEGFR/mTOR inhibitors were observed in ccRCC cell lines. In addition, according to the single-cell data,

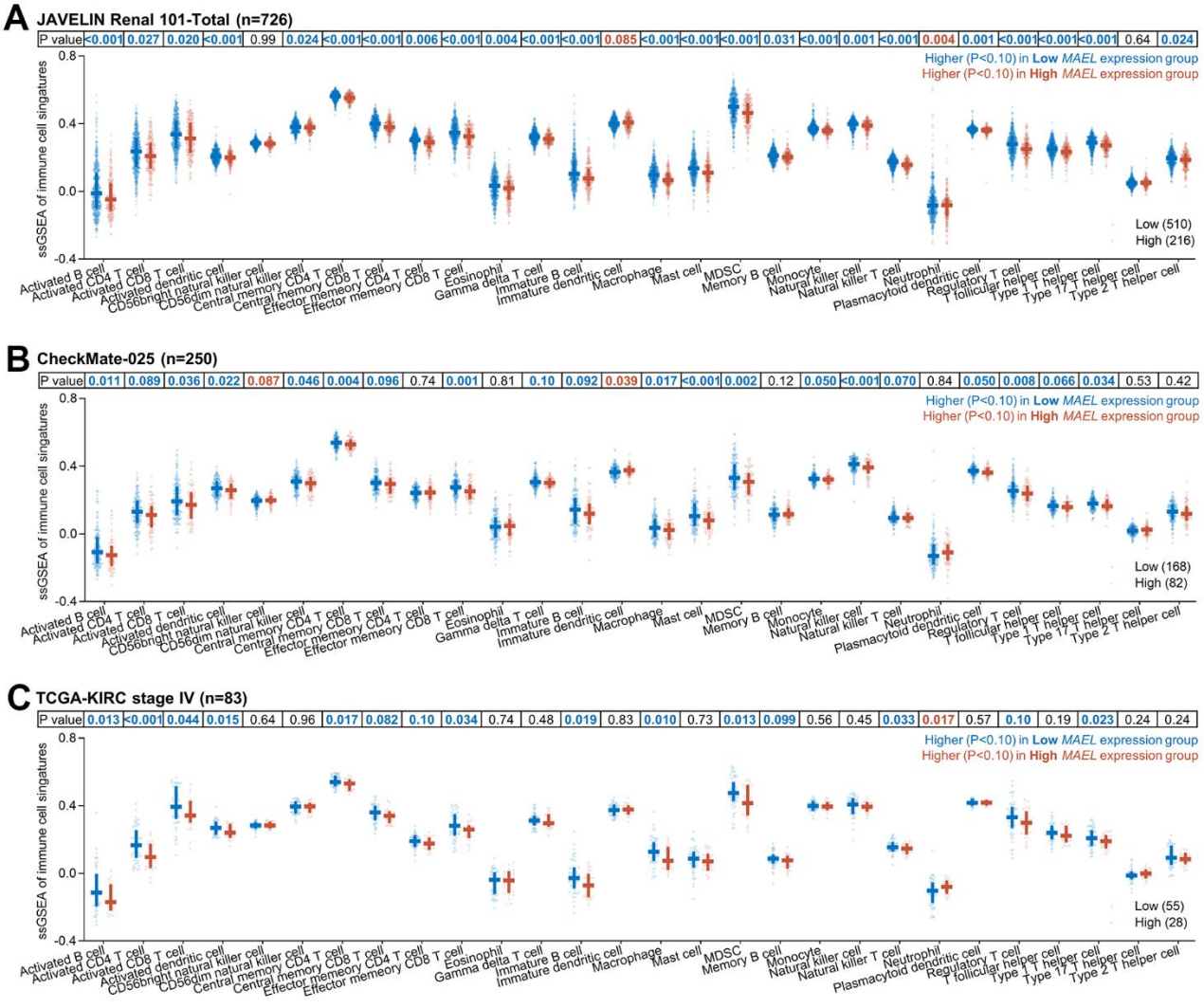

Figure 6. Association between *MAEL* expression and immune cell signatures in advanced/metastatic ccRCCs. (**A**–**C**) Association between *MAEL* expression and immune cell signatures in the JAVELIN Renal 101 cohort (**A**), the CheckMate-025 cohort (**B**), and the stage IV ccRCC patients in the TCGA-KIRC cohort (**C**). Abbreviations: MDSC=myeloid-derived suppressor cell, TCGA-KIRC=The Cancer Genome Atlas-Kidney Renal Clear Cell Carcinoma.

MAEL expression was undetectable in most of the peripheral blood mononuclear cells and the endothelial cells and fibroblasts in abdominal organs, suggesting that the results derived from tissue-bulk RNA data may reflect the characteristics of MAEL in ccRCC tumor cells instead of other cells, including endothelial cells, fibroblasts, and tumor-infiltrating immune cells. Second, the retrospective setting of our study may introduce biases, which can be minimized by the context of large randomized phase III trials and the implementation of multivariable analysis and independent validation. Third, the raw RNA-seq data from the public datasets are hard to obtain, so it's impossible to comprehensively analyzed the predictive utility of each *MAEL* transcript. Fortunately, the *MAEL* expression in ccRCCs was dominated by MAEL-206 (proportion>90%) and therefore our results based on the total *MAEL* expression can effectively reflect the effects of the dominant MAEL-202 in ccRCCs. Fourth, immune cell infiltration was estimated by ssGSEA in this study. Multiplex immunofluorescence of immune cell markers and MAEL in ccRCC samples would be beneficial for exploring the differences in tumor-infiltrating immune cells around *MAEL*-expressing and *MAEL*-non-expressing tumor cells. Fifth, the ICI regimens analyzed are avelumab plus axitinib and nivolumab monotherapy, which may represent anti-PD-(L)1 plus VEGFR inhibitor and anti-PD-(L)1 monotherapy, respectively. The combination of anti-PD-(L)1 and anti-CTLA-4 (e.g., CheckMate-214) was not included in our study due to the lack of patient-level data. Despite this, a negative association between *MAEL* expression and *CTLA-4* expression was observed in the two trials, suggesting the potential predictive utility of low *MAEL* expression for a large benefit from combination immunotherapy including anti-CTLA-4 over monotherapies of VEGFR/mTOR inhibitors.

To our knowledge, this is the first comprehensive analysis of *MAEL* in human cancers. High *MAEL* expression was observed in TGCT, glioma, pRCC, and ccRCC. Especially in ccRCC, *MAEL* is a biologically and clinically significant determinant with potential for prognostication after nephrectomy and patient selection for VEGFR/mTOR inhibitors and ICI-based immunotherapies. ICIs provide limited advantages and might not be strongly recommended for ccRCCs with high *MAEL* expression, by which the cost-effectiveness of treatments in ccRCCs may be potentially improved.

AUTHOR CONTRIBUTIONS

Conception and design: Jin Tao, Jinshan Cui, Yu Xu, and Yafeng Fan. Development of methodology: Yu Xu. Acquisition of data: Yu Xu. Analysis and interpretation of data: Yu Xu and Qiaoxia Zhou. Experiments: Yu Xu. Writing, review, and/or revision of the manuscript: Jin Tao, Jinshan Cui, Yu Xu, Yafeng Fan, Guodong Hong, Qiaoxia Zhou, Guoqiang Wang, Leo Li, Yusheng Han, Chunwei Xu, Wenxian Wang, Shangli Cai, Xuepei Zhang. Administrative, technical, or material support: Guoqiang Wang, Shangli Cai, Yusheng Han, and Xuepei Zhang. Study supervision: Xuepei Zhang. Final approval of manuscript: All authors.

ACKNOWLEDGMENTS

We thank Dizai Shi (Stitch) for his emotional support and the patients included and their family members for their understanding and participation.

CONFLICTS OF INTEREST

The authors declare no potential conflicts of interest, except the employment of Yu Xu, Qiaoxia Zhou, Guoqiang Wang, Leo Li, Yusheng Han, and Shangli Cai in Burning Rock Biotech.

FUNDING

This work was supported by 2018 Entrepreneurial Leading Talent of Guangzhou Huangpu District and Guangzhou Development District (2022-L023 to Yusheng Han).

REFERENCES

1. Clegg NJ, Frost DM, Larkin MK, Subrahmanyan L, Bryant Z, Ruohola-Baker H. maelstrom is required for an early step in the establishment of Drosophila oocyte polarity: posterior localization of grk mRNA. Development. 1997; 124:4661–71. https://doi.org/10.1242/dev.124.22.4661 PMID:9409682

2. Zhang D, Xiong H, Shan J, Xia X, Trudeau VL. Functional insight into Maelstrom in the germline piRNA pathway: a unique domain homologous to the DnaQ-H 3'-5' exonuclease, its lineage-specific expansion/loss and evolutionarily active site switch. Biol Direct. 2008; 3:48. https://doi.org/10.1186/1745-6150-3-48 PMID:19032786

3. Matsumoto N, Sato K, Nishimasu H, Namba Y, Miyakubi K, Dohmae N, Ishitani R, Siomi H, Siomi MC, Nureki O. Crystal Structure and Activity of the Endoribonuclease Domain of the piRNA Pathway Factor Maelstrom. Cell Rep. 2015; 11:366–75. https://doi.org/10.1016/j.celrep.2015.03.030 PMID:25865890

4. Chen KM, Campbell E, Pandey RR, Yang Z, McCarthy AA, Pillai RS. Metazoan Maelstrom is an RNA-binding

protein that has evolved from an ancient nuclease active in protists. RNA. 2015; 21:833–9. https://doi.org/10.1261/rna.049437.114 PMID:25778731

5. Xiao L, Wang Y, Zhou Y, Sun Y, Sun W, Wang L, Zhou C, Zhou J, Zhang J. Identification of a novel human cancer/testis gene MAEL that is regulated by DNA methylation. Mol Biol Rep. 2010; 37:2355–60. https://doi.org/10.1007/s11033-009-9741-x PMID:19693694

6. Kim SH, Park ER, Cho E, Jung WH, Jeon JY, Joo HY, Lee KH, Shin HJ. Mael is essential for cancer cell survival and tumorigenesis through protection of genetic integrity. Oncotarget. 2017; 8:5026–37. https://doi.org/10.18632/oncotarget.13756 PMID:27926513

7. Namba Y, Iwasaki YW, Nishida KM, Nishihara H, Sumiyoshi T, Siomi MC. Maelstrom functions in the production of Siwi-piRISC capable of regulating transposons in Bombyx germ cells. iScience. 2022; 25:103914. https://doi.org/10.1016/j.isci.2022.103914 PMID:35243263

8. Yuan L, Xiao Y, Zhou Q, Yuan D, Wu B, Chen G, Zhou J. Proteomic analysis reveals that MAEL, a component of nuage, interacts with stress granule proteins in cancer cells. Oncol Rep. 2014; 31:342–50. https://doi.org/10.3892/or.2013.2836 PMID:24189637

9. Gao X, Jiang L, Gong Y, Chen X, Ying M, Zhu H, He Q, Yang B, Cao J. Stress granule: A promising target for cancer treatment. Br J Pharmacol. 2019; 176:4421–33. https://doi.org/10.1111/bph.14790 PMID:31301065

10. Costa FF, Le Blanc K, Brodin B. Concise review: cancer/testis antigens, stem cells, and cancer. Stem Cells. 2007; 25:707–11. https://doi.org/10.1634/stemcells.2006-0469 PMID:17138959

11. Li P, Chen X, Qin G, Yue D, Zhang Z, Ping Y, Wang D, Zhao X, Song M, Zhao Q, Li J, Liu S, Wang D, et al. Maelstrom Directs Myeloid-Derived Suppressor Cells to Promote Esophageal Squamous Cell Carcinoma Progression via Activation of the Akt1/RelA/IL8 Signaling Pathway. Cancer Immunol Res. 2018; 6:1246–59. https://doi.org/10.1158/2326-6066.CIR-17-0415 PMID:30082413

12. Zhang X, Ning Y, Xiao Y, Duan H, Qu G, Liu X, Du Y, Jiang D, Zhou J. MAEL contributes to gastric cancer progression by promoting ILKAP degradation. Oncotarget. 2017; 8:113331–44. https://doi.org/10.18632/oncotarget.22970 PMID:29371914

13. Li Q, Wei P, Huang B, Xu Y, Li X, Li Y, Cai S, Li D. MAEL expression links epithelial-mesenchymal transition and stem cell properties in colorectal cancer. Int J Cancer. 2016; 139:2502–11. https://doi.org/10.1002/ijc.30388 PMID:27537253

14. Liu L, Dai Y, Chen J, Zeng T, Li Y, Chen L, Zhu YH, Li J, Li Y, Ma S, Xie D, Yuan YF, Guan XY. Maelstrom promotes hepatocellular carcinoma metastasis by inducing epithelial-mesenchymal transition by way of Akt/GSK-3β/Snail signaling. Hepatology. 2014; 59:531–43. https://doi.org/10.1002/hep.26677 PMID:23929794

15. He WP, Yang GP, Yang ZX, Shen HW, You ZS, Yang GF. Maelstrom promotes tumor metastasis through regulation of FGFR4 and epithelial-mesenchymal transition in epithelial ovarian cancer. J Ovarian Res. 2022; 15:55. https://doi.org/10.1186/s13048-022-00992-4 PMID:35513870

16. Li XD, Zhang JX, Jiang LJ, Wang FW, Liu LL, Liao YJ, Jin XH, Chen WH, Chen X, Guo SJ, Zhou FJ, Zeng YX, Guan XY, et al. Overexpression of maelstrom promotes bladder urothelial carcinoma cell aggressiveness by epigenetically downregulating MTSS1 through DNMT3B. Oncogene. 2016; 35:6281–92. https://doi.org/10.1038/onc.2016.165 PMID:27181205

17. Karlsson M, Zhang C, Méar L, Zhong W, Digre A, Katona B, Sjöstedt E, Butler L, Odeberg J, Dusart P, Edfors F, Oksvold P, von Feilitzen K, et al. A single-cell type transcriptomics map of human tissues. Sci Adv. 2021; 7:eabh2169. https://doi.org/10.1126/sciadv.abh2169 PMID:34321199

18. Thul PJ, Åkesson L, Wiking M, Mahdessian D, Geladaki A, Ait Blal H, Alm T, Asplund A, Björk L, Breckels LM, Bäckström A, Danielsson F, Fagerberg L, et al. A subcellular map of the human proteome. Science. 2017; 356:eaal3321. https://doi.org/10.1126/science.aal3321 PMID:28495876

19. Uhlen M, Karlsson MJ, Zhong W, Tebani A, Pou C, Mikes J, Lakshmikanth T, Forsström B, Edfors F, Odeberg J, Mardinoglu A, Zhang C, von Feilitzen K, et al. A genome-wide transcriptomic analysis of protein-coding genes in human blood cells. Science. 2019; 366:eaax9198. https://doi.org/10.1126/science.aax9198 PMID:31857451

20. Liu J, Lichtenberg T, Hoadley KA, Poisson LM, Lazar AJ, Cherniack AD, Kovatich AJ, Benz CC, Levine DA, Lee AV, Omberg L, Wolf DM, Shriver CD, et al, and Cancer Genome Atlas Research Network. An Integrated TCGA

Pan-Cancer Clinical Data Resource to Drive High-Quality Survival Outcome Analytics. Cell. 2018; 173:400–16.e11. https://doi.org/10.1016/j.cell.2018.02.052 PMID:29625055

21. Tang Z, Kang B, Li C, Chen T, Zhang Z. GEPIA2: an enhanced web server for large-scale expression profiling and interactive analysis. Nucleic Acids Res. 2019; 47:W556–60. https://doi.org/10.1093/nar/gkz430 PMID:31114875

22. Koch A, De Meyer T, Jeschke J, Van Criekinge W. MEXPRESS: visualizing expression, DNA methylation and clinical TCGA data. BMC Genomics. 2015; 16:636. https://doi.org/10.1186/s12864-015-1847-z PMID:26306699

23. Koch A, Jeschke J, Van Criekinge W, van Engeland M, De Meyer T. MEXPRESS update 2019. Nucleic Acids Res. 2019; 47:W561–5. https://doi.org/10.1093/nar/gkz445 PMID:31114869

24. Lang H, Béraud C, Bethry A, Danilin S, Lindner V, Coquard C, Rothhut S, Massfelder T. Establishment of a large panel of patient-derived preclinical models of human renal cell carcinoma. Oncotarget. 2016; 7:59336–59. https://doi.org/10.18632/oncotarget.10659 PMID:27449081

25. Peña-Llopis S, Vega-Rubín-de-Celis S, Liao A, Leng N, Pavía-Jiménez A, Wang S, Yamasaki T, Zhrebker L, Sivanand S, Spence P, Kinch L, Hambuch T, Jain S, et al. BAP1 loss defines a new class of renal cell carcinoma. Nat Genet. 2012; 44:751–9. https://doi.org/10.1038/ng.2323 PMID:22683710

26. Thorsson V, Gibbs DL, Brown SD, Wolf D, Bortone DS, Ou Yang TH, Porta-Pardo E, Gao GF, Plaisier CL, Eddy JA, Ziv E, Culhane AC, Paull EO, et al, and Cancer Genome Atlas Research Network. The Immune Landscape of Cancer. Immunity. 2018; 48:812–30.e14. https://doi.org/10.1016/j.immuni.2018.03.023 PMID:29628290

27. ICGC/TCGA Pan-Cancer Analysis of Whole Genomes Consortium. Pan-cancer analysis of whole genomes. Nature. 2020; 578:82–93. https://doi.org/10.1038/s41586-020-1969-6 PMID:32025007

28. Calabrese C, Davidson NR, Demircioğlu D, Fonseca NA, He Y, Kahles A, Lehmann KV, Liu F, Shiraishi Y, Soulette CM, Urban L, Greger L, Li S, et al, PCAWG Transcriptome Core Group, PCAWG Transcriptome Working Group, and PCAWG Consortium. Genomic basis for RNA alterations in cancer. Nature. 2020; 578:129–36. https://doi.org/10.1038/s41586-020-1970-0 PMID:32025019

29. Yang W, Soares J, Greninger P, Edelman EJ, Lightfoot H, Forbes S, Bindal N, Beare D, Smith JA, Thompson IR, Ramaswamy S, Futreal PA, Haber DA, et al. Genomics of Drug Sensitivity in Cancer (GDSC): a resource for therapeutic biomarker discovery in cancer cells. Nucleic Acids Res. 2013; 41:D955–61. https://doi.org/10.1093/nar/gks1111 PMID:23180760

30. Beuselinck B, Job S, Becht E, Karadimou A, Verkarre V, Couchy G, Giraldo N, Rioux-Leclercq N, Molinié V, Sibony M, Elaidi R, Teghom C, Patard JJ, et al. Molecular subtypes of clear cell renal cell carcinoma are associated with sunitinib response in the metastatic setting. Clin Cancer Res. 2015; 21:1329–39. https://doi.org/10.1158/1078-0432.CCR-14-1128 PMID:25583177

31. Motzer RJ, Escudier B, McDermott DF, George S, Hammers HJ, Srinivas S, Tykodi SS, Sosman JA, Procopio G, Plimack ER, Castellano D, Choueiri TK, Gurney H, et al, and CheckMate 025 Investigators. Nivolumab versus Everolimus in Advanced Renal-Cell Carcinoma. N Engl J Med. 2015; 373:1803–13. https://doi.org/10.1056/NEJMoa1510665 PMID:26406148

32. Vivian J, Rao AA, Nothaft FA, Ketchum C, Armstrong J, Novak A, Pfeil J, Narkizian J, Deran AD, Musselman-Brown A, Schmidt H, Amstutz P, Craft B, et al. Toil enables reproducible, open source, big biomedical data analyses. Nat Biotechnol. 2017; 35:314–6. https://doi.org/10.1038/nbt.3772 PMID:28398314

33. Cunningham F, Allen JE, Allen J, Alvarez-Jarreta J, Amode MR, Armean IM, Austine-Orimoloye O, Azov AG, Barnes I, Bennett R, Berry A, Bhai J, Bignell A, et al. Ensembl 2022. Nucleic Acids Res. 2022; 50:D988–95. https://doi.org/10.1093/nar/gkab1049 PMID:34791404

34. Mi H, Muruganujan A, Ebert D, Huang X, Thomas PD. PANTHER version 14: more genomes, a new PANTHER GO-slim and improvements in enrichment analysis tools. Nucleic Acids Res. 2019; 47:D419–26. https://doi.org/10.1093/nar/gky1038 PMID:30407594

35. Gene Ontology Consortium. The Gene Ontology resource: enriching a GOld mine. Nucleic Acids Res. 2021; 49:D325–34. https://doi.org/10.1093/nar/gkaa1113 PMID:33290552

36. Subramanian A, Tamayo P, Mootha VK, Mukherjee S, Ebert BL, Gillette MA, Paulovich A, Pomeroy SL, Golub TR, Lander ES, Mesirov JP. Gene set enrichment analysis: a knowledge-based approach for interpreting genome-wide expression profiles. Proc Natl Acad Sci USA. 2005; 102:15545–50.

https://doi.org/10.1073/pnas.0506580102
PMID:16199517

37. Liu XD, Kong W, Peterson CB, McGrail DJ, Hoang A, Zhang X, Lam T, Pilie PG, Zhu H, Beckermann KE, Haake SM, Isgandrova S, Martinez-Moczygemba M, et al. PBRM1 loss defines a nonimmunogenic tumor phenotype associated with checkpoint inhibitor resistance in renal carcinoma. Nat Commun. 2020; 11:2135.
https://doi.org/10.1038/s41467-020-15959-6
PMID:32358509

38. Dizman N, Philip EJ, Pal SK. Genomic profiling in renal cell carcinoma. Nat Rev Nephrol. 2020; 16:435–51.
https://doi.org/10.1038/s41581-020-0301-x
PMID:32561872

39. Konishi S, Hatakeyama S, Tanaka T, Ikehata Y, Tanaka T, Fujita N, Ishibashi Y, Yamamoto H, Yoneyama T, Hashimoto Y, Yoshikawa K, Kawaguchi T, Masumori N, et al. Comparison of axitinib and sunitinib as first-line therapies for metastatic renal cell carcinoma: a real-world multicenter analysis. Med Oncol. 2018; 36:6.
https://doi.org/10.1007/s12032-018-1231-3
PMID:30474747

40. Motzer RJ, Hutson TE, Glen H, Michaelson MD, Molina A, Eisen T, Jassem J, Zolnierek J, Maroto JP, Mellado B, Melichar B, Tomasek J, Kremer A, et al. Lenvatinib, everolimus, and the combination in patients with metastatic renal cell carcinoma: a randomised, phase 2, open-label, multicentre trial. Lancet Oncol. 2015; 16:1473–82.
https://doi.org/10.1016/S1470-2045(15)00290-9
PMID:26482279

41. Hutson TE, Lesovoy V, Al-Shukri S, Stus VP, Lipatov ON, Bair AH, Rosbrook B, Chen C, Kim S, Vogelzang NJ. Axitinib versus sorafenib as first-line therapy in patients with metastatic renal-cell carcinoma: a randomised open-label phase 3 trial. Lancet Oncol. 2013; 14:1287–94.
https://doi.org/10.1016/S1470-2045(13)70465-0
PMID:24206640

42. Jonasch E, Walker CL, Rathmell WK. Clear cell renal cell carcinoma ontogeny and mechanisms of lethality. Nat Rev Nephrol. 2021; 17:245–61.
https://doi.org/10.1038/s41581-020-00359-2
PMID:33144689

43. McDermott DF, Huseni MA, Atkins MB, Motzer RJ, Rini BI, Escudier B, Fong L, Joseph RW, Pal SK, Reeves JA, Sznol M, Hainsworth J, Rathmell WK, et al. Clinical activity and molecular correlates of response to atezolizumab alone or in combination with bevacizumab versus sunitinib in renal cell carcinoma. Nat Med. 2018; 24:749–57.
https://doi.org/10.1038/s41591-018-0053-3
PMID:29867230

44. Braun DA, Hou Y, Bakouny Z, Ficial M, Sant' Angelo M, Forman J, Ross-Macdonald P, Berger AC, Jegede OA, Elagina L, Steinharter J, Sun M, Wind-Rotolo M, et al. Interplay of somatic alterations and immune infiltration modulates response to PD-1 blockade in advanced clear cell renal cell carcinoma. Nat Med. 2020; 26:909–18.
https://doi.org/10.1038/s41591-020-0839-y
PMID:32472114

45. Liu K, Huang Y, Xu Y, Wang G, Cai S, Zhang X, Shi T. BAP1-related signature predicts benefits from immunotherapy over VEGFR/mTOR inhibitors in ccRCC: a retrospective analysis of JAVELIN Renal 101 and checkmate-009/010/025 trials. Cancer Immunol Immunother. 2023; 72:2557–72.
https://doi.org/10.1007/s00262-023-03424-4
PMID:37046008

46. Ballman KV. Biomarker: Predictive or Prognostic? J Clin Oncol. 2015; 33:3968–71.
https://doi.org/10.1200/JCO.2015.63.3651
PMID:26392104

47. Cancer Genome Atlas Research Network. Comprehensive molecular characterization of clear cell renal cell carcinoma. Nature. 2013; 499:43–9.
https://doi.org/10.1038/nature12222
PMID:23792563

48. Wang Y, Fu D, Chen Y, Su J, Wang Y, Li X, Zhai W, Niu Y, Yue D, Geng H. G3BP1 promotes tumor progression and metastasis through IL-6/G3BP1/STAT3 signaling axis in renal cell carcinomas. Cell Death Dis. 2018; 9:501.
https://doi.org/10.1038/s41419-018-0504-2
PMID:29717134

49. Motzer RJ, Choueiri TK, McDermott DF, Powles T, Vano YA, Gupta S, Yao J, Han C, Ammar R, Papillon-Cavanagh S, Saggi SS, McHenry MB, Ross-Macdonald P, Wind-Rotolo M. Biomarker analysis from CheckMate 214: nivolumab plus ipilimumab versus sunitinib in renal cell carcinoma. J Immunother Cancer. 2022; 10:e004316.
https://doi.org/10.1136/jitc-2021-004316
PMID:35304405

50. Motzer RJ, Banchereau R, Hamidi H, Powles T, McDermott D, Atkins MB, Escudier B, Liu LF, Leng N, Abbas AR, Fan J, Koeppen H, Lin J, et al. Molecular Subsets in Renal Cancer Determine Outcome to Checkpoint and Angiogenesis Blockade. Cancer Cell. 2020; 38:803–17.e4.
https://doi.org/10.1016/j.ccell.2020.10.011
PMID:33157048

SUPPLEMENTARY MATERIALS

Supplementary Methods

Human protein atlas (HPA) RNA-seq data of normal tissue and blood samples

For normal tissue and blood samples, specimens were collected with consent from patients and all samples were anonymized in accordance with approval from the local ethics committee (ref #2011/473 and ref #2015/1552-32) and Swedish rules and legislation. All tissues were collected from the Uppsala Biobank and RNA samples were extracted from frozen tissue sections. Blood samples were enriched for PBMC and granulocytes, labeled with antibodies and separated into subpopulation by flow sorting. mRNA sequencing was performed on Illumina HiSeq2000 and 2500 machines (Illumina, San Diego, CA, USA) using the standard Illumina RNA-seq protocol with a read length of 2x100 bases. Blood cells mRNA sequencing was performed on an Illumina NovaSeq 6000 System in four S4 lanes with a read length of 2x150 bases. Transcript abundance estimation was performed using Kallisto v0.46.2. The 18 blood cell types are classified into six different lineages including B-cells, T-cells, NK-cells, monocytes, granulocytes, and dendritic cells.

The HPA Human brain sample set contains 1324 samples of >200 regions of the human brain. The analysis is a collaboration with Human Brain Tissue Bank (HBTB; Semmelweis University, Budapest) in accordance with approval from the Committee of Science and Research Ethic of the Ministry of Health Hungary (ETT TUKEB: 189/KO/02.6008/2002/ETT) and the Semmelweis University Regional Committee of Science and Research Ethic (No. 32/1992/TUKEB) to remove human brain tissue samples, collect, store and use them for research. Samples were collected by Prof. Palkovits and RNA was extracted from frozen brain punches. The human prefrontal cortex dataset includes 165 samples from 3 male and 3 female donors providing a detailed overview of protein expression in 17 subregions of the prefrontal cortex and 3 reference cortical regions was analyzed using the Illumina sequencing platform, all other samples were analyzed using the MGI DNBSEQ-T7 platform.

For more detail, please see https://www.proteinatlas.org/about/assays+annotation#hpa_rna.

Single cell RNA-seq data

The single cell RNA sequencing dataset is based on meta-analysis of literature on single cell RNA sequencing and single cell databases that include healthy human tissue. To avoid technical bias and to ensure that the single cell dataset can best represent the corresponding tissue, the following data selection criteria were applied: (1) Single cell transcriptomic datasets were limited to those based on the Chromium single cell gene expression platform from 10X Genomics (version 2 or 3); (2) Single cell RNA sequencing was performed on single cell suspension from tissues without pre-enrichment of cell types; (3) Only studies with >4,000 cells and 20 million read counts were included; (4) Only dataset whose pseudo-bulk transcriptomic expression profile is highly correlated with the transcriptomic expression profile of the corresponding HPA tissue bulk sample were included. It should be noted that exceptions were made for lung (~7.3 million reads), pancreas (3,719 cells) and rectum (3,898 cells) to include various cell types in the analysis.

In total, single cell transcriptomics data for 25 tissues and peripheral blood mononuclear cells (PBMCs) were analyzed. These datasets were respectively retrieved from the Single Cell Expression Atlas, the Human Cell Atlas, the Gene Expression Omnibus, the Allen Brain Map, and the European Genome-phenome Archive. The complete list of references is shown in Supplementary Table 2.

For each of the single cell transcriptomics datasets, the quantified raw sequencing data were downloaded from the corresponding depository database based on the accession number provided by the corresponding study in the available format (total cells, read, and feature counts, or count tables). Unfiltered data were used as input for downstream analysis with an in-house pipeline using Scanpy (version 1.4.4.post1) in Python 3.7.3 for the 13 tissues and PBMC published in HPA v20 and Scanpy (version 1.7.2) in Python 3.8.5 for the 12 tissues published in HPA v21. In the pipeline, the data were filtered using two criteria: a cell is considered as valid if at least 200 genes are detected and a gene is considered as valid if it is expressed in at least 10% of the cells. Specially, in the HPA v21, tissues which contain more than 10,000 cells used 1000 cells as their cutoff. Subsequently, the cell counts were normalized to have a total count per cell of 10000. The valid cells were then clustered using Louvain clustering function within Single-Cell Analysis in Python (Scanpy). Default values of parameters were used in clustering. More in detail, the features of cells were projected into a PCA space with 50 components using UMAP, and a k-nearest neighbours (KNN) graph was generated. 15 neighbours were used in the network for Louvain, while

the resolution of clustering was set as 1.0. The total read counts for all genes in each cluster was calculated by adding up the read counts of each gene in all cells belonging to the corresponding cluster. Finally, the read counts were normalized to transcripts per million protein coding genes (pTPM) for each of the single cell clusters. When calculating the expression profile for pseudo-bulk samples based on single cell transcriptomics, we added the read counts for all genes from all cells of the sample, and normalized it to pTPM in the same way as for the cluster ones.

Each of the 444 different cell type clusters were manually annotated based on an extensive survey of >500 well-known tissue and cell type-specific markers, including both markers from the original publications, and additional markers used in pathology diagnostics. For each cluster, one main cell type was chosen by taking into consideration the expression of different markers. For a few clusters, no main cell type could be selected, and these clusters were not used for gene classification. The most relevant markers are presented in a heatmap on the Cell Type Atlas, in order to clarify cluster annotation to visitors.

The cell type dendrogram presented on the Single Cell Type section shows the relationship between the single cell types based on genome-wide expression. The dendrogram is based on agglomerative clustering of 1 - Spearman's rho between cell types using Ward's criterion. The dendrogram was then transformed into a hierarchical graph, and link distances were normalized to emphasize graph connections rather than link distances. Link width is proportional to the distance from the root, and links are colored according to cell type group if only one cell type group is present among connected leaves.

For more detail, please see https://www.proteinatlas.org/about/assays+annotation#singlecell_rna.

Supplementary Figures

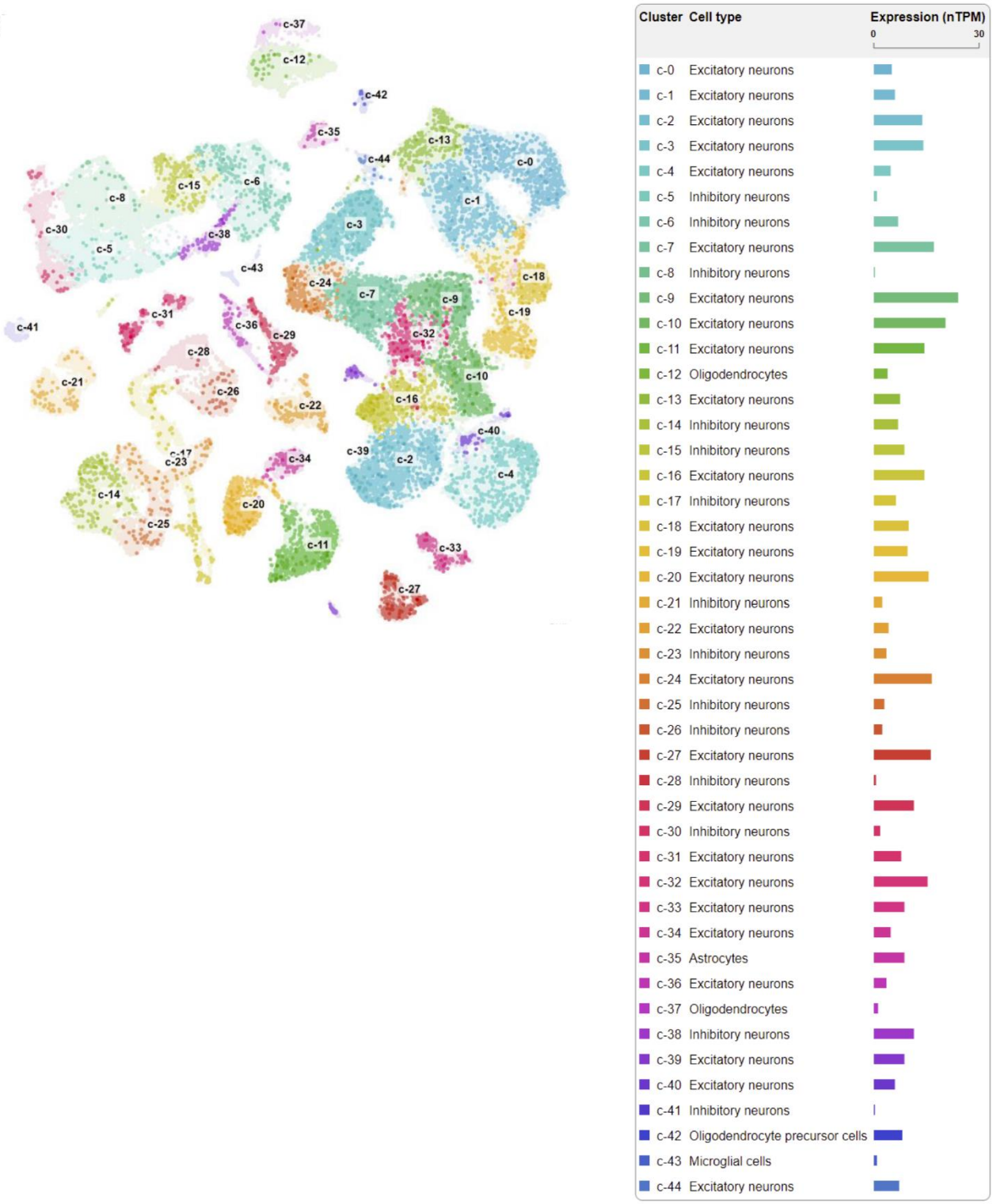

Supplementary Figure 1. UMAP plot and *MAEL* expression in the single cell clusters of normal brain (Allen brain map).

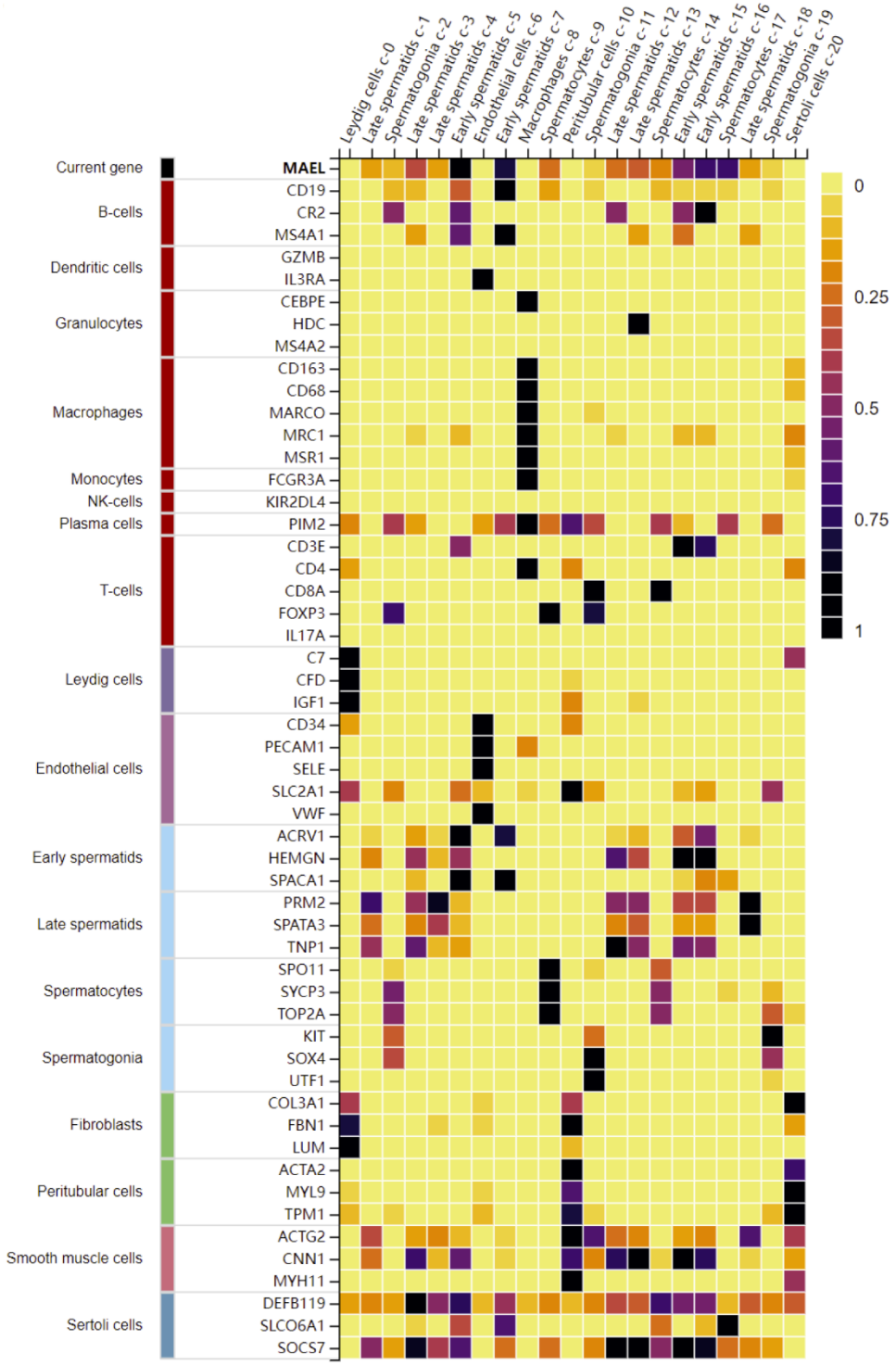

Supplementary Figure 2. mRNA expression of *MAEL* and cell type markers in different single cell type clusters of normal testis (GSE120508). Color legend: fraction of the highest expression.

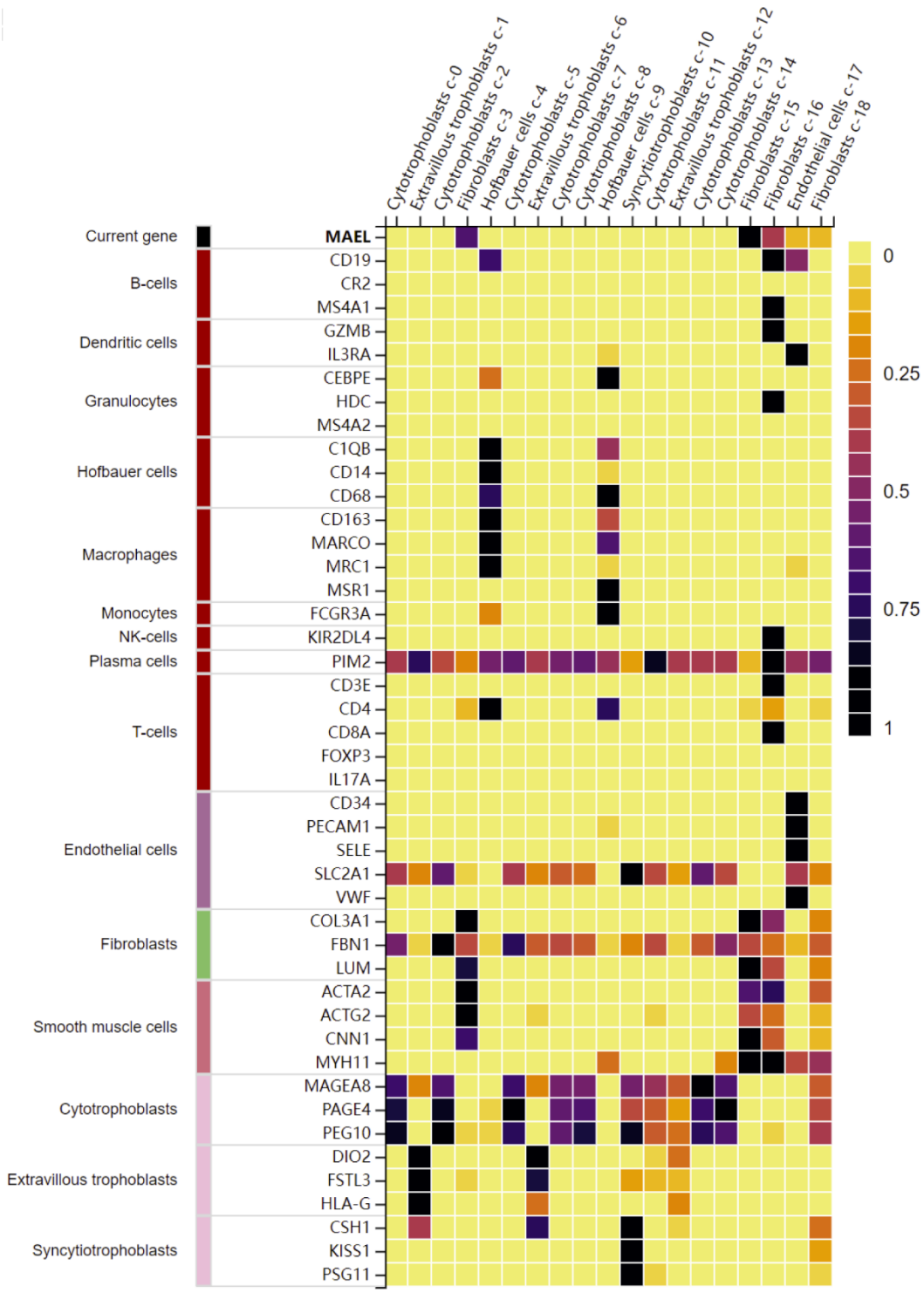

Supplementary Figure 3. mRNA expression of *MAEL* and cell type markers in different single cell type clusters of normal placenta (E-MTAB-6701). Color legend: fraction of the highest expression.

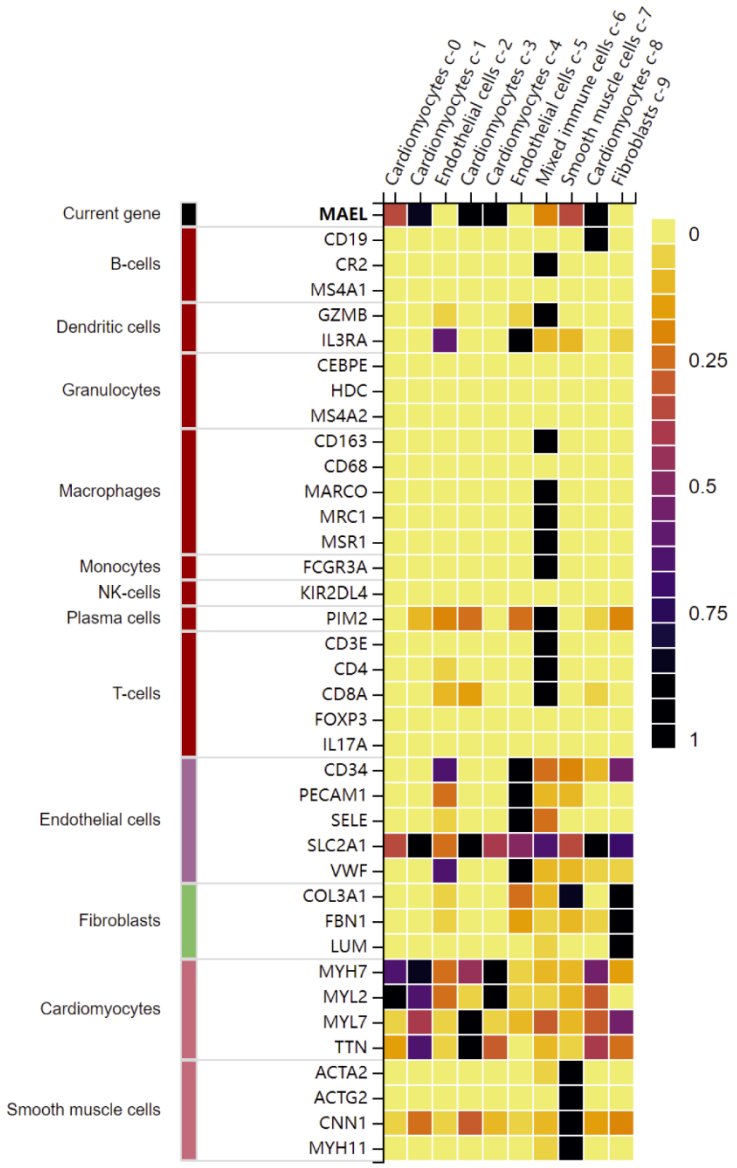

Supplementary Figure 4. mRNA expression of *MAEL* and cell type markers in different single cell type clusters of normal heart muscle (GSE109816). Color legend: fraction of the highest expression.

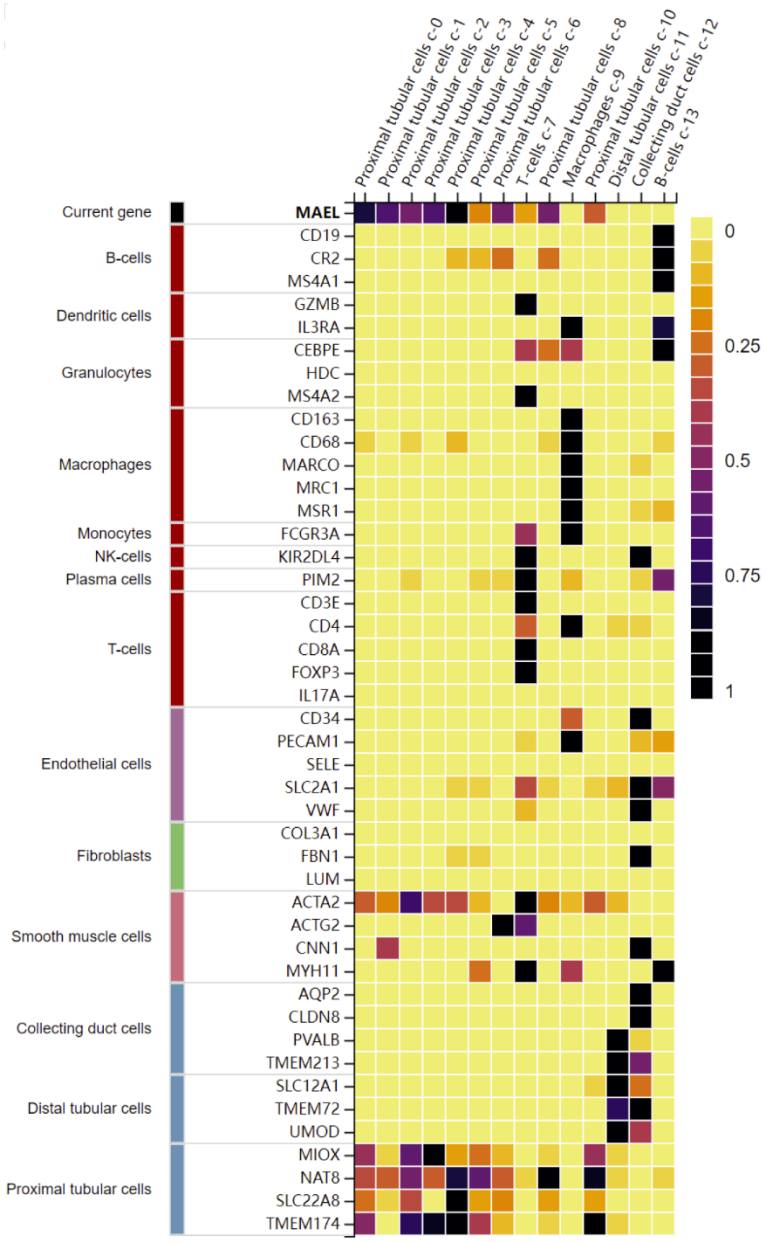

Supplementary Figure 5. mRNA expression of *MAEL* and cell type markers in different single cell type clusters of normal kidney (GSE131685). Color legend: fraction of the highest expression.

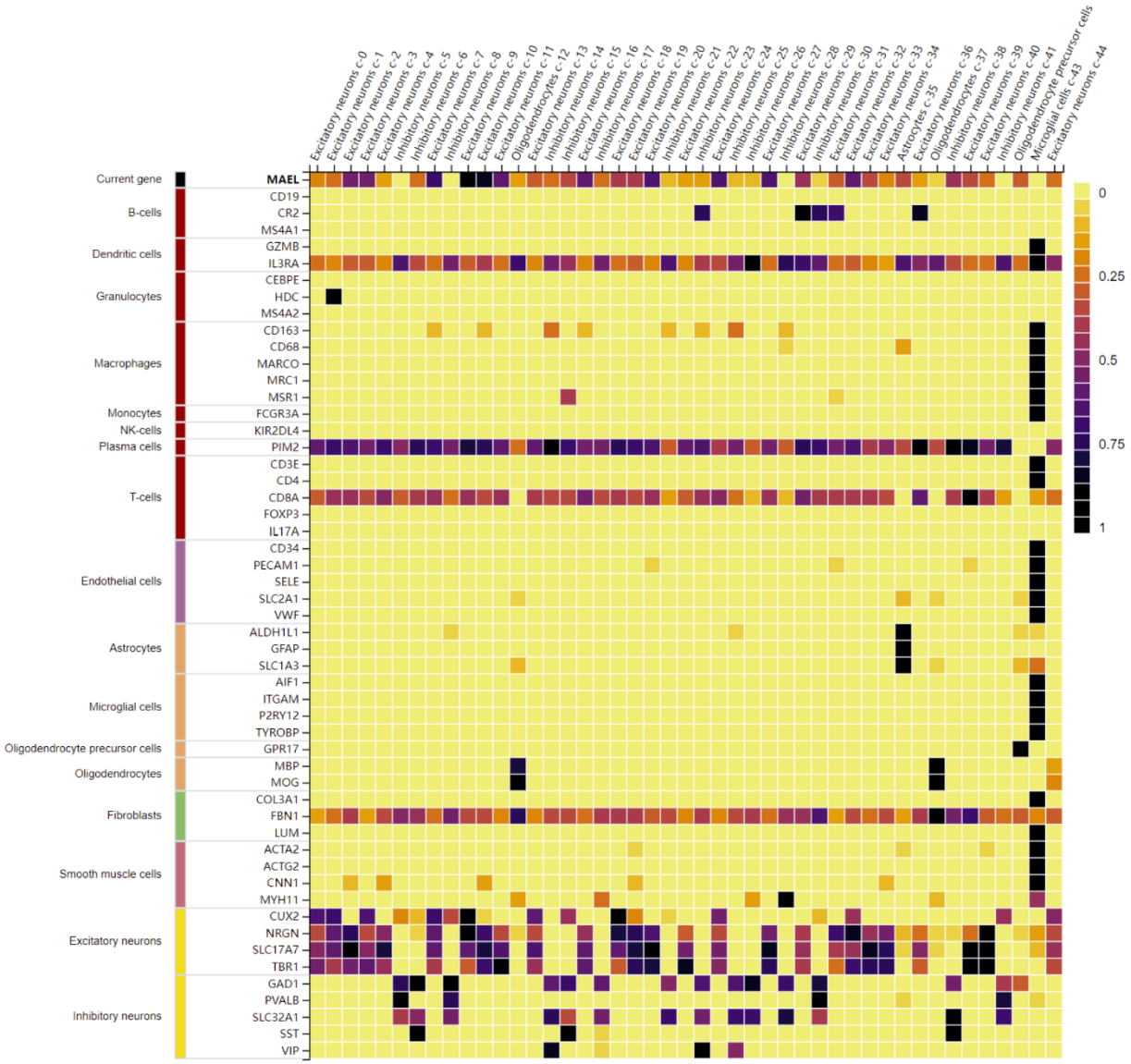

Supplementary Figure 6. mRNA expression of *MAEL* and cell type markers in different single cell type clusters of normal brain (Allen brain map). Color legend: fraction of the highest expression.

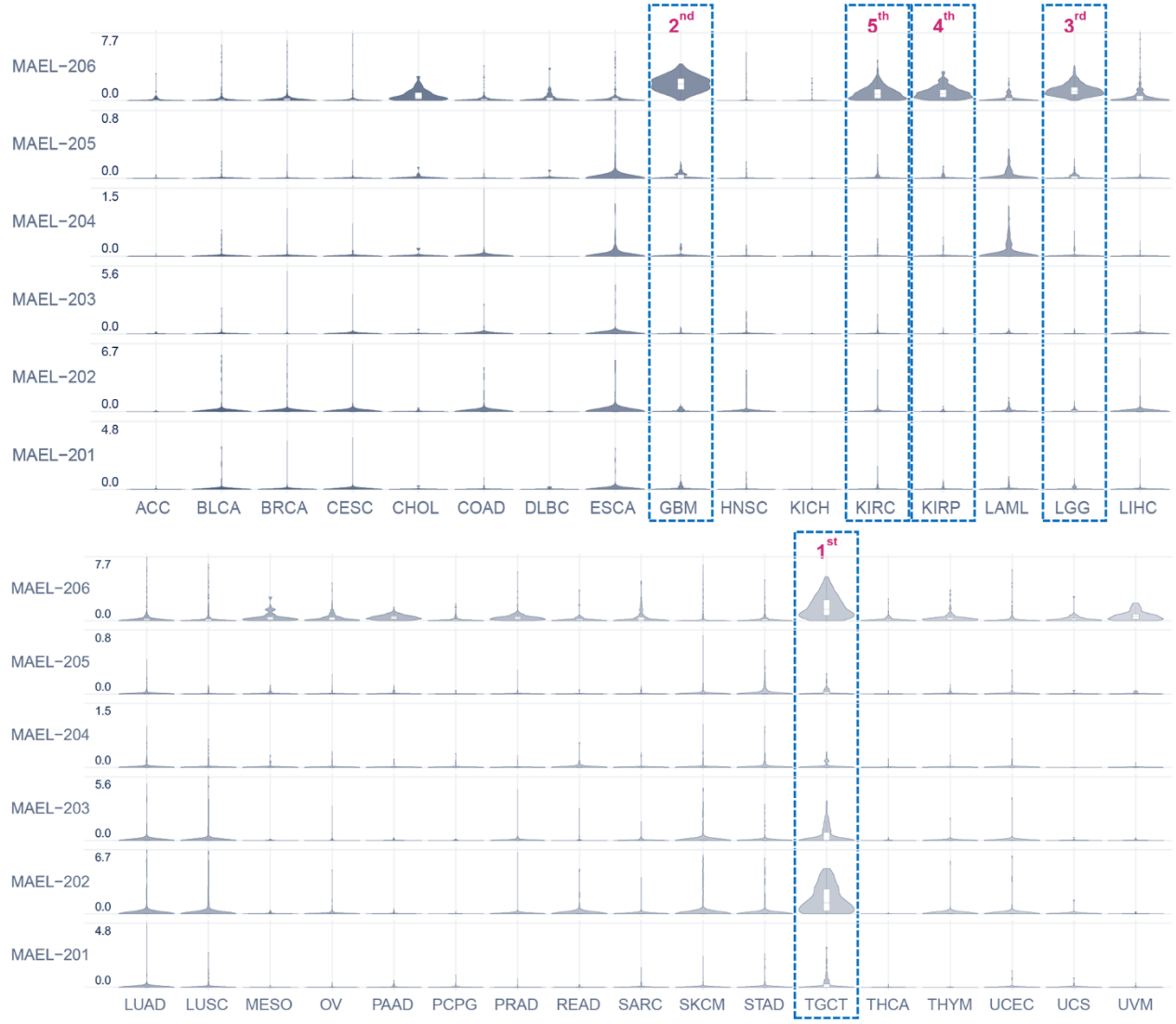

Supplementary Figure 7. mRNA expression of the six transcripts of *MAEL* among 33 types of cancer (unit: log2[TPM+1]).

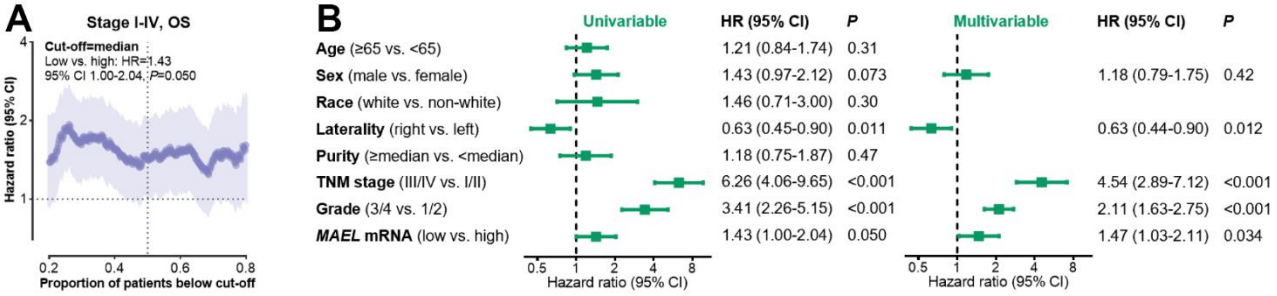

Supplementary Figure 8. Association between *MAEL* expression and recurrence-free survival in the clear cell renal cell carcinomas of the TCGA-KIRC cohort.

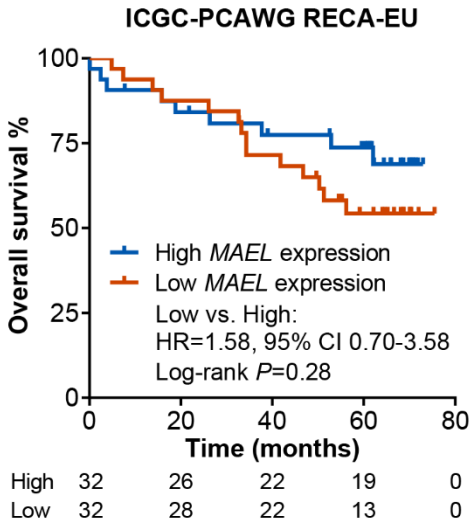

Supplementary Figure 9. Association between *MAEL* expression and overall survival in the clear cell renal cell carcinomas of the ICGC-PCAWG RECA-EU cohort.

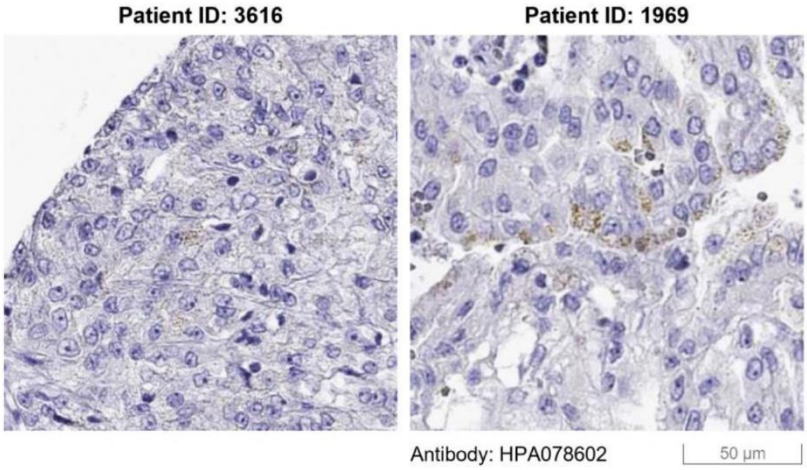

Supplementary Figure 10. Immunohistochemical staining of *MAEL* in ccRCC samples.

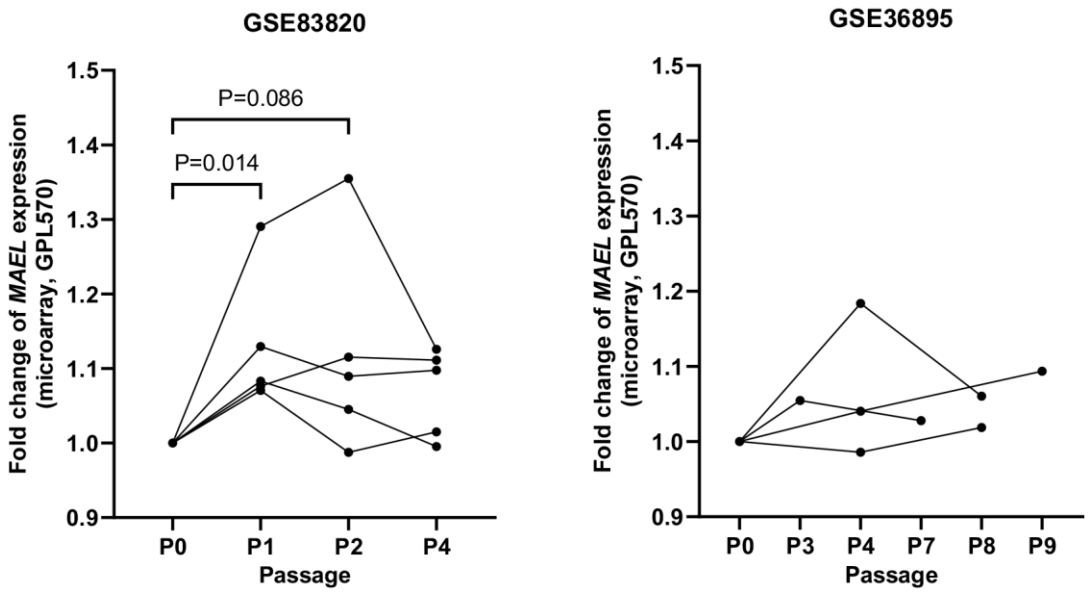

Supplementary Figure 11. Expression of *MAEL* in ccRCC xenograft models.

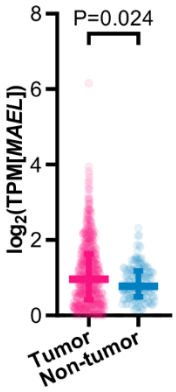

Supplementary Figure 12. *MAEL* expression in clear cell renal cell carcinomas (TCGA-KIRC) and normal kidneys (TCGA-KIRC and GTEx).

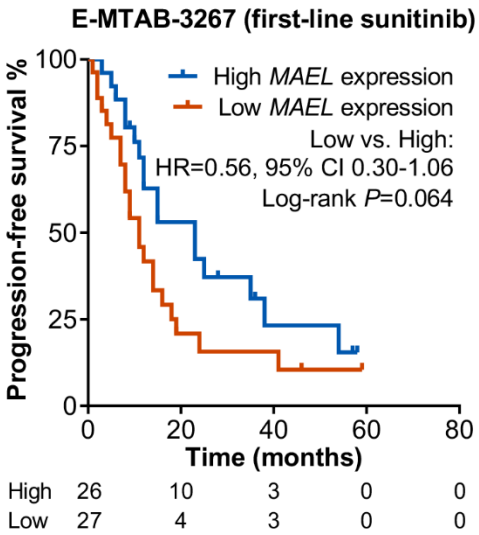

Supplementary Figure 13. High *MAEL* expression was associated with favorable progression-free survival on first-line sunitinib in advanced clear cell renal cell carcinomas (E-MTAB-3267).

Supplementary Tables

Please browse Full Text version to see the data of Supplementary Tables 3, 4, 8, 9.

Supplementary Table 1. Single cell transcriptomics datasets.

Tissue	Data source	No. of M reads	No. of cells	Correlation with HPA bulk RNA	Reference
Colon	GSE116222	12.9	11167	0.811	Parikh K et al. (2019)
Eye	GSE137537	22.6	20091		Menon M et al. (2019)
Heart muscle	GSE109816	396.7	9182	0.797	Wang L et al. (2020)
Small intestine	GSE125970	59.6	6167		Wang Y et al. (2020)
Kidney	GSE131685	56.2	25279	0.867	Liao J et al. (2020)
Liver	GSE115469	42	8439	0.837	MacParland SA et al. (2018)
Lung	GSE130148	6.9	4599	0.863	Vieira Braga FA et al. (2019)
Placenta	E-MTAB-6701	347	18547	0.879	Vento-Tormo R et al. (2018)
Prostate	GSE117403	177.4	35862	0.756	Henry GH et al. (2018)
Rectum	GSE125970	60.4	3898	0.756	Wang Y et al. (2020)
PBMC	GSE112845	19.4	4972	0.756	Chen J et al. (2018)
Testis	GSE120508	70.5	6490	0.756	Guo J et al. (2018)
Pancreas	GSE131886	92.3	3719	0.829	Qadir MMF et al. (2020)
Skin	GSE130973	56.4	15798	0.756	Solé-Boldo L et al. (2020)
Brain		1357.2	76533	0.661	Allen brain map
Bronchus		85.3	17521		Lukassen S et al. (2020)
Endometrium	GSE111976	624.1	71032	0.807	Wang W et al. (2020)
Skeletal muscle	GSE143704	77.8	22030	0.697	De Micheli AJ et al. (2020)
Ovary	GSE146512	259.2	43636	0.808	Man L et al. (2020)
Adipose tissue	GSE155960	418.5	83536	0.813	Hildreth AD et al. (2021)
Esophagus	159929-GSM4850580	31.5	9117	0.84	He S et al. (2020)
Lymph node	GSE159929-GSM4850583	14.2	7771	0.849	He S et al. (2020)
Bone marrow	GSE159929-GSM4850584	8.6	3230	0.818	He S et al. (2020)
Spleen	GSE159929-GSM4850589	14.8	4512	0.804	He S et al. (2020)
Stomach	GSE159929-GSM4850590	18.9	5318	0.814	He S et al. (2020)
Breast	GSE164898	342.3	47662	0.839	Bhat-Nakshatri P et al. (2021)

Supplementary Table 2. Basic characteristics of the included dataset.

	TCGA-KIRC	ICGC-PCAWG RECA-EU	GDSC	JAVELIN Renal 101	CM-025	E-MTAB-3267	GSE83820	GSE36895
Number of patients/cell lines with mRNA data	522	64	16	726	250	53	5	4
Data used in the present study	Mutation, copy number variation, mRNA, lncRNA, clinicopathological data, OS	mRNA, OS	mRNA, IC50	mRNA, PFS	mRNA, PFS	mRNA, PFS	mRNA	mRNA
Sequencing method of transcriptomic	RNA-seq	RNA-seq	RNA-seq (Illumina HiSeq 2000 or HiSeq 2500)	RNA-seq (Illumina HiSeq 2500)	RNA-seq (Illumina HiSeq 2000 or HiSeq 2500)	Microarray (GPL6244)	Microarray (GPL570)	Microarray (GPL570)
PD-L1 immunohistochemical staining	NA	NA	NA	SP142, immune cell score	NA	NA	NA	NA
Therapy	NA	NA	Targeted agents	Avelumab+Axitinib vs. Sunitinib (1st line)	Nivolumab vs. Everolimus (2nd-3rd line)	Sunitinib (1st line)	NA	NA

Abbreviations: ICGC-PCAWG RECA-EU, International Cancer Genome Consortium-Pan-cancer analysis of whole genomes Renal Cell Carcinoma-Europe; OS, overall survival; PFS, progression-free survival.

Supplementary Table 3. *MAEL* expression in normal tissues.

Supplementary Table 4. Single cell transcriptomics.

Supplementary Table 5. Abbreviations in the TCGA and the CCLE databases.

Abbreviations	Full name	TCGA	CCLE
ACC	Adrenocortical carcinoma	√	
ALL	Acute lymphocytic leukemia		√
BLCA	Bladder urothelial carcinoma	√	√
BRCA	Breast invasive carcinoma	√	√
CESC	Cervical squamous cell carcinoma and endocervical adenocarcinoma	√	√
CLL	Chronic lymphocytic leukemia		√
CHOL	Cholangiocarcinoma	√	
COAD	Colon adenocarcinoma	√	√
DLBC	Diffuse large B cell lymphoma	√	√
ESCA	Esophageal carcinoma	√	√
	Ewings sarcoma		√
GBM	Glioblastoma multiforme	√	√
HNSC	Head and neck squamous cell carcinoma	√	√
KICH	Kidney chromophobe	√	
KIRC	Kidney renal clear cell carcinoma	√	√
KIRP	Kidney renal papillary cell carcinoma	√	
LAML	Acute myeloid leukemia	√	√
LCML	Chronic myelogenous leukemia		√
LGG	Brain lower grade glioma	√	√
LIHC	Liver hepatocellular carcinoma	√	√
LUAD	Lung adenocarcinoma	√	√
LUSC	Lung squamous cell carcinoma	√	√
MB	Medulloblastoma		√
MESO	Mesothelioma	√	√
MM	Multiple myeloma		√
NB	Neuroblastoma		√
NSCLC	Non-small cell lung cancer		√
OV	Ovarian serous cystadenocarcinoma	√	√
PAAD	Pancreatic adenocarcinoma	√	√
PCPG	Pheochromocytoma and paraganglioma	√	
PRAD	Prostate adenocarcinoma	√	√
READ	Rectal adenocarcinoma	√	√
SARC	Sarcoma	√	√
SCLC	Small cell lung cancer		√
SKCM	Skin cutaneous melanoma	√	√
STAD	Stomach adenocarcinoma	√	√
TGCT	Testicular germ cell tumor	√	
THCA	Thyroid carcinoma	√	√
THYM	Thymoma	√	
UCEC	Uterine corpus endometrial carcinoma	√	√
UCS	Uterine carcinosarcoma	√	
UVM	Uveal melanoma	√	

Supplementary Table 6. Features of the six transcripts of *MAEL*.

Transcript ID	Name	bp	Protein	Translation ID	Biotype	CCDS	UniProt match	RefSeq match
ENST00000367870.6	MAEL-201	1831	403aa	ENSP00000356844.2	Protein coding	CCDS65712	Q96JY0-2	-
ENST00000367872.9	MAEL-202	1737	434aa	ENSP00000356846.4	Protein coding	CCDS1257	Q96JY0-1	NM_032858.3
ENST00000447624.1	MAEL-203	1013	316aa	ENSP00000402143.1	Protein coding		X6RGB1	-
ENST00000487826.1	MAEL-204	416	No protein	-	Processed transcript		-	-
ENST00000491055.5	MAEL-205	2355	No protein	-	Processed transcript		-	-
ENST00000622874.4	MAEL-206	1700	378aa	ENSP00000482771.1	Protein coding	CCDS72975	E9JVC4	-

Supplementary Table 7. Associations of *MAEL* expression with clinicopathological features, copy number variations, and DNA methylation.

Variable	KIRC		TGCT	
	P-value	Pearson r	P-value	Pearson r
Age	0.426483266825387	-0.0324428362771666	0.752333563410853	0.0270047807184707
Sex	0.0904257180696398	NA	NA	NA
Race	0.194246293049914	NA	0.872982066854064	NA
Histological grade	0.021952312664529	NA	9.56399423005252E-07	0.40542915383908
Pathological T	0.135787374901966	NA	0.177488104232116	NA
Pathologic N	0.225732314323571	NA	0.958850252206529	NA
Pathological M	0.103451317195837	NA	NA	NA
Tumor stage	0.0639348682885934	NA	0.229241921454448	NA
Copy number variation	0.0000124053286982694	0.190110076688231	0.752916482313235	-0.0259154877503306
cg13081288	0.000785685953360897	-0.180743238710894	0.0000628585334375174	-0.314957369168476
cg08348962	0.0492590402535173	-0.108009393639065	0.243763849009391	-0.0938743944622001
cg18323210	0.092512587133264	-0.0911124474315059	0.5440767694976	0.0489361999183405
cg03758693	NA	NA	NA	NA
cg11503720	0.352805528905452	0.0503959163684299	0.480610749333206	0.0568827237605001
cg15965055	0.529796595162321	0.034090418549852	0.0315425603321009	0.172254607829556
cg22603542	0.409987244359549	0.0446936912631353	0.186481189999048	-0.106325340667379
cg07725889	NA	NA	NA	NA
cg10117884	0.897947345270261	0.00696064119958166	3.94858256423742E-09	-0.452757600333627
cg18894878	0.920711985278922	-0.00540209688290252	6.52822637100908E-16	-0.610024898231754
cg27053975	0.435695401537689	0.0422856006668722	2.99438405154888E-15	-0.596408048402836
cg24453820	0.301857453783545	-0.0559901939447633	8.67166538012812E-17	-0.627691428644751
cg23968893	0.896436555610462	-0.00706426328384486	1.84345878539201E-15	-0.60077299206138
cg11336590	0.66528813578229	-0.0236158222038295	3.53364947237034E-19	-0.673975652934597
cg19241352	0.0828312211934396	-0.0939273014761928	1.11483104794639E-18	-0.664515504411586
cg13480774	0.709249632452788	0.0202341815113491	1.49945009591534E-15	-0.602623339738763
cg24586196	0.212520272989992	-0.0675823337211926	2.40573208547595E-16	-0.618813017897356
cg00001349	0.28226677455352	-0.0583064319125126	1.2178606809646E-12	-0.539768091814994
cg13249256	0.283087524604477	-0.0582072645293623	6.21117501997563E-19	-0.669344119897905
cg17757848	0.84317847389987	-0.0107363993229523	2.95924429682114E-19	-0.675427522082466
cg13212575	0.969169533256836	0.00209763722753289	3.17730546470227E-16	-0.616374517921076
cg26308818	0.596084245542656	0.0287606442778004	3.39217204532824E-07	-0.396023176042178

Supplementary Table 8. Correlation between the mRNA expression of *MAEL* and other genes.

Supplementary Table 9. Original IC50 and transformed IC50 of the 16 ccRCC cell lines.